



Defense Intelligence Reference Document

Defense Futures

11 January 2011

ICOD: 10 August 2010

DIA-08-1102-007

Quantum Tomography of Negative Energy States in the Vacuum

Quantum Tomography of Negative Energy States in the Vacuum

The **Defense Intelligence Reference Document** provides non-substantive but authoritative reference information related to intelligence topics or methodologies.

Prepared by:

(b)(3):10 USC 424

Defense Intelligence Agency

Author:

(b)(6)

COPYRIGHT WARNING: Further dissemination of the photographs in this publication is not authorized.

This product is one of a series of advanced technology reports produced in FY 2010 under the Defense Intelligence Agency, (b)(3):10 USC 424 Advanced Aerospace Weapons System Applications (AAWSA) Program. Comments or questions pertaining to this document should be addressed to

(b)(3):10 USC 424;(b)(6) AAWSA Program Manager, Defense Intelligence Agency, ATTN: (b)(3):10 USC 424

(b)(3):10 USC 424 Bldg. 6000, Washington D.C. 20340-5100.

Contents

Introduction	1
REVIEW OF NEGATIVE (or SUB-VACUUM) ENERGY	3
Overview	3
Examples of Negative (Sub-Vacuum) Energy Found in Nature	4
Basic Notions of the Quantum Field Theory of Light	5
Basic Notions on the Origin of the Quantum Vacuum Zero-Point	
Fluctuations	7
Negative (Sub-Vacuum) Energy in Squeezed Light	8
Negative (Sub-Vacuum) Energy in the Casimir Effect.....	13
QUANTUM OPTICAL HOMODYNE TOMOGRAPHY.....	15
Observing Negative Energy in the Lab.....	15
Basic Notions of Quantum Optical Homodyne Tomography	16
Wigner Functions	17
Beam Splitters.....	24
Photodiodes	27
Balanced Homodyne Detection	27
Outline of Experimental Procedure.....	32
BALANCED HOMODYNE SYSTEMS FOR MEASURING NEGATIVE	
(SUB-VACUUM) ENERGY	33
Time-Domain Balanced Homodyne System	33
Balanced Homodyne System for Casimir Cavities	36
CONCLUSION.....	43
ACKNOWLEDGEMENTS	45
REFERENCES	46

Figures

Figure 1. Illustration of a Squeezed State of Light 13
Figure 2. Schematic of the Casimir Effect 14
Figure 3. Illustration of Quantum Optical Homodyne Tomography 16
Figure 4. Wigner Function for a Vacuum and for a Coherent State 19
Figure 5. Wigner Function of a Squeezed Vacuum..... 20
Figure 6. Wigner Function of a Single Photon..... 21
Figure 7. Quantum Tomography of Schrödinger-Cat States..... 22
Figure 8. Schematic of an Ideal Lossless Beam Splitter..... 25
Figure 9. Illustration of a Fictitious Beam Splitter..... 26
Figure 10. Schematic of a Balanced Homodyne Detector..... 29
Figure 11. Balanced Homodyne Detector Using Fictitious Beam Splitters..... 31
**Figure 12. Balanced Homodyne Detector Using A Single Effective Fictitious Beam
Splitter 32**
Figure 13. Time-Domain Balanced Homodyne Detector..... 34
Figure 14. Experimentally Measured Squeezed State 35
Figure 15. Balanced Homodyne Detector with a Local Oscillator 38
Figure 16. Diagram of Casimir Cavity with BHD Photodiodes 40
Figure 17. Experimental Setup of BHD Photodiodes and LO Field 40
Figure 18. Detailed Schematic of Experimental BHD Apparatus 41
Figure 19. Predicted Casimir Spectral Density..... 41
Figure 20. Predicted Suppression of Vacuum Fluctuations in dB. 42

Quantum Tomography of Negative Energy States in the Vacuum

Introduction

Future aerospace vehicles could have an advanced propulsion system that uses negative quantum vacuum energy to modify the spacetime geometry in the immediate vicinity surrounding the vehicle in order to induce faster-than-light motion via traversable wormholes or warp drives, or even levitation via antigravity [1, 2]. These exotic propulsion concepts are well-known in mainstream general relativity and quantum field theory research. The notion of a physical state with negative energy is not familiar in the realm of classical physics. However, it is not rare in quantum field theory to have quantum states with negative energy density or a negative energy flux. Even for a quantum scalar field in the flat Minkowski spacetime, it can be proved that the existence of quantum states with negative energy density is inevitable [3].

Although all known forms of classical matter have non-negative energy density, it is not so in quantum field theory. A general quantum state can be a superposition of particle number eigenstates and may have a negative expectation value of energy density in certain spacetime regions due to quantum coherence effects [3]. These considerations remain true even for quantum fields in a curved spacetime where the effects of gravitational fields, or equivalently, accelerations, can be observed due to the mass of astronomical bodies or the motions of astronomical bodies.

There are two key examples of specially prepared quantum vacuum states that are known to produce small amounts of negative energy density in the laboratory. These are the well-known Casimir effect and the squeezed vacuum states of the electromagnetic field. The former is a static quantum vacuum effect while the latter is a time-domain quantum vacuum effect. There are several other examples of special quantum vacuum or particle states that produce negative energy density, but they are beyond the scope of this report because they remain mathematical curiosities or are not practicable to implement in the laboratory in the foreseeable future.

We already make small amounts of negative energy in the laboratory via the Casimir effect and squeezed electromagnetic vacuum states, but we do not yet know if we can access larger amounts for extended periods of time over extended spatial distributions for the purpose of modifying spacetime for aerospace propulsion applications. It will be necessary to first explore the quantum nature of the Casimir effect and squeezed electromagnetic vacuum states to determine whether we can measure and spatially map their negative energy density. This is a necessary first step to take before beginning any study on producing large quantities of negative energy because we will first need to know how to measure and spatially map negative energy in order to properly control it after producing it. This is the motivation for this report.

We need to firm up our understanding of how lab detectors will respond to negative energy *in situ*. A first step in this direction was already taken by Hansen et al. [4] in 2001 for the time-domain negative energy pulses in squeezed electromagnetic vacuum states, and more recently Marecki [5, 6] generalized the analysis of the output of balanced homodyne detectors (BHDs) for the case of static negative energy states

inside Casimir cavities. The most important feature of these devices is their ability to quantify the quantum vacuum fluctuations of the electric field because the output of BHDs provides information on the one- and two-point functions of arbitrary states of quantum fields. Marecki computed the two-point function and the associated spectral density for the ground state of the quantum electric field in Casimir geometries, and predicts a position- and frequency-dependent pattern of BHD responses if a device of this type is placed inside a Casimir cavity. The proposed device allows for the direct detection of quantum vacuum fluctuations and provides a spatial mapping of the negative energy contained inside the cavity, which will be summarized in this report.

REVIEW OF NEGATIVE (or SUB-VACUUM) ENERGY

Overview

The implementation of faster-than-light (FTL) interstellar travel via traversable wormholes or warp drives or other antigravity forces for propulsion, generally requires the engineering of spacetime into very specialized local geometries surrounding the immediate vicinity of the aerospace vehicle undergoing this type of motion. The analysis of these via the general relativistic field equation plus the resultant source matter equations of state demonstrates that such geometries require the use of "exotic" matter in order to produce the requisite FTL or antigravity spacetime modification. Exotic matter is generally defined by general relativity physics to be matter that possesses (renormalized) negative energy density (sometimes negative stress-tension = outward pressure, a.k.a. gravitational repulsion or antigravity), and this is a very misunderstood and misapplied term by the non-general relativity community. We clear up this misconception by defining what negative energy is, where it can be found in nature, and we also review the two primary experimental concepts that are known to produce negative energy in the laboratory. Also, it has been claimed that FTL and antigravity spacetimes are not plausible because exotic matter violates the general relativistic energy conditions. However, it has been shown that this is a spurious issue. The identification, magnitude, and production of exotic matter is seen to be a key technical challenge, however. FTL and antigravity spacetimes also possess features that challenge the notions of causality and there are alleged constraints placed upon them by quantum effects. Reference [1] reviews and summarizes these issues with an assessment on the present state of their resolution.

What exactly is "exotic" matter? In classical physics the energy density of all observed forms of matter (fields) is non-negative. What is exotic about the type of matter that must be used to produce traversable wormhole, warp drive, or antigravity spacetimes is that it must have negative energy density and/or negative flux [7]. The energy density is "negative" in the sense that the configuration of matter fields we must deploy to produce a traversable wormhole, warp drive, or antigravity effect must have an energy density, $\rho_E (= \rho c^2$, where ρ is the rest-mass density), that is less than or equal to its pressures/tensions, p_i [8, 9].* In many cases, these equations of state are also known to possess an energy density that is algebraically negative, i.e., the energy density and flux are less than zero. It is on the basis of these conditions that we call this material property "exotic." The condition for ordinary, classical (non-exotic) forms of matter that we are all familiar with in nature is that $\rho_E > p_i$ and/or $\rho_E \geq 0$. These conditions represent two examples of what are variously called the "standard" energy conditions which are computed from the trace of the matter stress-energy tensor[†]: Weak Energy Condition (WEC: $\rho_E \geq 0$, $\rho_E + p_i \geq 0$), Null Energy Condition (NEC: $\rho_E + p_i \geq 0$), Dominant Energy Condition (DEC), and Strong Energy Condition (SEC). These energy conditions forbid negative energy density between material objects to occur in nature, but they are mere hypotheses. Hawking and Ellis [10] formulated the energy conditions in order to establish a series of mathematical hypotheses governing the behavior of

* From this point forward, all Latin letters (e.g., $i, j, k = 1..3$) that appear as indices on physical quantities denote the usual 3-dimensional space coordinates, $x^1..x^3$, indicating the spatial components of vector or tensor quantities.

[†] The stress-energy-momentum tensor is a matrix quantity that encodes the density and flux of energy and momentum for any type of matter under study.

collapsed-matter singularities in their study of cosmology and black hole physics. More specifically, classical general relativity allows one to prove lots of general theorems about the behavior of matter in gravitational fields.

However, real physical matter is not “reasonable” because the energy conditions are in general violated by semiclassical quantum effects (occurring at order η) [9].[†] More specifically, quantum effects generically violate the average NEC (ANEC). Furthermore, it was discovered in 1965 that quantum field theory has the remarkable property of allowing states of matter containing local regions of negative energy density or negative fluxes [3]. This violates the WEC, which postulates that the local energy density is non-negative for all observers. And there are also general theorems of differential geometry that guarantee that there must be a violation of one, some, or all of the energy conditions (meaning exotic matter is present) for all FTL and antigravity spacetimes. However, all of the energy condition hypotheses have been experimentally tested in the laboratory and experimentally shown to be false – 25 years before their formulation [11].

In quantum field theory, negative energy is a manifestation of what is now called the “sub-vacuum” levels of the quantum zero-point (or vacuum ground state) fluctuations that correspond to any particular quantum field of matter under study. Hence, the energy corresponding to sub-vacuum quantum fluctuations is now called “sub-vacuum energy”: sub-vacuum energy \equiv negative energy. Further investigation into this technical issue showed that violations of the energy conditions are widespread for all forms of both “reasonable” classical and quantum matter [12-16]. Furthermore, Visser [9] showed that all (generic) spacetime geometries violate all the energy conditions. So the condition that $\rho_E > p_i$ and/or $\rho_E \geq 0$ must be obeyed by all forms of matter in nature is spurious. Negative energy has been produced in the laboratory and this will be discussed in the following sections.

Examples of Negative (Sub-Vacuum) Energy Found in Nature

The exotic (energy condition-violating) fields that are known to occur in nature are:

1. Static, radially-dependent electric or magnetic fields. These are borderline exotic, if their tension were infinitesimally larger, for a given energy density [10, 17].
2. Squeezed quantum vacuum states: electromagnetic and other (non-Maxwellian) quantum fields [8, 18].
3. Gravitationally squeezed electromagnetic vacuum fluctuations [19].
4. Casimir effect, i.e., the Casimir vacuum in flat, curved, and topological spaces [20-28].
5. Other quantum fields/states/effects. In general, the local energy density in quantum field theory can be negative due to quantum coherence effects [3]. Other examples that have been studied are Dirac field states: the superposition of two single particle electron states and the superposition of two multi-electron-positron states [29, 30]. In the former (latter), the energy densities can be negative when two single (multi-) particle states have the same number of

[†] Planck’s reduced constant, $\eta = 1.055 \times 10^{-34}$ J·s.

electrons (electrons and positrons) or when one state has one more electron (electron-positron pair) than the other.

Cosmological inflation [9], cosmological particle production [9], classical scalar fields [9], the conformal anomaly [9], and gravitational vacuum polarization [12-15] are among many other examples that also violate the energy conditions. Since the laws of quantum field theory place no strong restrictions on negative energies and fluxes, then it might be possible to produce exotic phenomena such as faster-than-light travel [31-33], traversable wormholes [8, 9, 34], violations of the second law of thermodynamics [35, 36], and time machines [9, 34, 37]. There are several other exotic phenomena made possible by the effects of negative energy, but they lie outside the scope of this report. In what follows, we consider only items 2 and 4 in the previous list for the purpose of this report due to their ready applicability and technical maturity. We will not examine the other items in the list because they are theoretical curiosities that remain under study by investigators.

Basic Notions of the Quantum Field Theory of Light

Before going further, it will be helpful to briefly outline the basic notions and terminology of the quantum field theory of light (i.e., quantum optics) because the content of this report focuses on those aspects.

Classically, light is electromagnetic radiation that can be pictured as waves flowing through space at the speed of light, c ($= 3.0 \times 10^8$ m/s). The waves are not waves of anything substantive, but are in fact ripples in the state of a field. These waves carry energy, and each wave has a specific direction, frequency and polarization state. This is called a "propagating mode of the electromagnetic field." A simple model for this is the electromagnetic oscillator. One complex-valued vector function $u(x,t)$ called a spatial-temporal mode comprises all classical wave aspects including polarization. The simplest example of a spatial-temporal mode is a plane wave

$u(x,t) = u_0 \exp[i(kx - \omega t)]$ of polarization vector u_0 , angular frequency ω , and wave vector k (definition: $k^2 = \omega^2/c^2$), where i is the unit complex number, and x is the space coordinate and t is the time coordinate.

This mode defines a framework in space and time that may be excited by the quantum field "light." The mode function quantifies the strength of one excitation in space and time. Also, the mode function obeys the laws of classical waves given by Maxwell's equations of electrodynamics. The choice of $u(x,t)$ is made by the observer. The observer singles out one mode, one quantum object from the rest of the world to make a specific observation or measurement. This object turns out to be a harmonic oscillator described by the annihilation operator \hat{a} . A useful tool for modeling the propagating mode of the electromagnetic field in quantum mechanics is the ideal quantum mechanical harmonic oscillator: a hypothetical charged mass on a perfect spring oscillating back and forth under the action of the spring's restoring force. The operator \hat{a} stands for the quantized amplitude with which $u(x,t)$ can be excited. In classical optics it would be just a complex number α of magnitude $|\alpha|$ and phase $\arg(\alpha)$. The quantized amplitude \hat{a} is neither predetermined nor given by the observer

but depends on the state of $u(x,t)$. This state exists even if literally nothing is in the mode chosen by the observer. In this case, the light is just in the *vacuum state*.[§] However, this “nothing” can indeed cause significant physical effects as will be discussed in later sections.

To make all this more precise, we postulate that the electric field strength \hat{E} of the light field is given by $\hat{E} = u^*(x,t)\hat{a} + u(x,t)\hat{a}^\dagger$ and that the amplitude operator \hat{a} is a bosonic** annihilation operator that obeys the quantum mechanical commutation relation $[\hat{a}, \hat{a}^\dagger] = 1$, where $u^*(x,t)$ is the complex conjugate of $u(x,t)$ and \hat{a}^\dagger is the adjoint (or conjugate) of \hat{a} called the creation operator.^{††} The hat symbol appearing over quantities denotes that they are quantum operators (or observables). Another key element of quantum-oscillator physics is the photon number operator \hat{n} , which accounts for the number of photons (quantized light particles) in the chosen $u(x,t)$ and is given by the quantum mechanical counterpart of a classical modulus-squared amplitude: $\hat{n} \equiv \hat{a}^\dagger \hat{a}$.

Let us now introduce a pair of operators, \hat{q} and \hat{p} , called quadratures. They are defined as $\hat{q} = 2^{-1/2}(\hat{a}^\dagger + \hat{a})$ and $\hat{p} = i2^{-1/2}(\hat{a}^\dagger - \hat{a})$, which can be inverted to provide the additional useful definitions $\hat{a} = 2^{-1/2}(\hat{q} + i\hat{p})$ and $\hat{a}^\dagger = 2^{-1/2}(\hat{q} - i\hat{p})$. In optics \hat{q} and \hat{p} correspond to the in-phase and the out-of-phase component of the electric field amplitude of $u(x,t)$ (with respect to a reference phase). The bosonic commutation relation demonstrates that \hat{q} and \hat{p} are canonically conjugate observables, $[\hat{q}, \hat{p}] = i\hbar$. The quadratures \hat{q} and \hat{p} can be regarded as the position and the momentum of the quantum electromagnetic oscillator. They do not appear in real space but in the phase space spanned by the complex vibrational amplitude \hat{a} of the quantum electromagnetic oscillator, and they have nothing to do with the position and the momentum of a photon. However, the canonical commutation relation entitles us to treat \hat{q} and \hat{p} as perfect examples of position- and momentum-like quantities in quantum optics. Finally, we express the photon number operator \hat{n} in terms of the quadratures \hat{q} and \hat{p} and obtain, using the bosonic commutation relation, the standard Hamiltonian (or total energy) of the quantum harmonic (electromagnetic) oscillator with unit mass and frequency:

$$\begin{aligned} \hat{H}_{\text{osc}} &\equiv \hat{n} + \frac{1}{2} \\ &= \frac{\hat{p}^2}{2} + \frac{\hat{q}^2}{2}, \end{aligned} \tag{1}$$

[§] Here we always mean by “vacuum” simply “no light” and not an evacuated system.

** Boson or bosonic refers to quantum particles that have integer quantum spin.

†† In quantum mechanics, the vacuum is defined to be a state of no (or zero) particles and is denoted by the quantum state eigenvector $|0\rangle$. By definition \hat{a} “annihilates” the vacuum state: $\hat{a}|0\rangle = 0$.

where the first and second terms in the second line are the kinetic and potential energies of the oscillator, respectively. The additional $1/2$ appearing in the first line of Eq. (1) is called the *vacuum zero-point energy* for the reason to be explained in the next section. The first line of Eq. (1) is more commonly expressed in units of energy (Joules) in quantum mechanics, which is obtained simply by multiplying the right-hand side by the photon energy $\hbar\omega$ so that $\hat{H}_{\text{osc}} = \hbar\omega\left(\hat{n} + \frac{1}{2}\right)$.

It is beyond the scope of this report to elaborate further on the entire subject of the quantum optics. The reader should consult Reference [38] for more information.

Basic Notions on the Origin of the Quantum Vacuum Zero-Point Fluctuations

Here we discuss the basic notions of the quantum vacuum zero-point fluctuations (ZPF), which is an important feature in quantum optics. The origin of the ZPF is attributed to the Heisenberg Uncertainty Principle. According to this principle, \hat{q} and \hat{p} are any two conjugate observables that we are interested in measuring, and they obey the commutation relation already shown in the previous section. Their corresponding uncertainty relation is $\Delta\hat{q}\Delta\hat{p} \geq \hbar/2$, where $\Delta\hat{q}$ is the variance (a.k.a. uncertainty) of observable \hat{q} and $\Delta\hat{p}$ is that of the conjugate observable \hat{p} . This relation states that if one measures observable \hat{q} with very high precision (i.e., its uncertainty $\Delta\hat{q}$ is very small), then a simultaneous measurement of observable \hat{p} will be less precise (i.e., its uncertainty $\Delta\hat{p}$ is very large), and vice versa. In other words, it is not possible to simultaneously measure two conjugate observable quantities with infinite precision.

This minimum uncertainty is not due to any correctable flaws in measurement, but rather reflects the intrinsic fuzziness in the quantum nature of energy and matter. Substantial theoretical and experimental work has shown that in many quantum systems the limits to measurement precision is imposed by the quantum vacuum ZPF embodied within the uncertainty principle. Nowadays we rather see the Heisenberg Uncertainty Principle as a necessary consequence, and therefore, a derived result of the wave nature of quantum phenomena. The uncertainties are just a consequence of the Fourier nature of conjugate pairs of quantities (observables). For example, the two Fourier-wave-conjugates time and frequency become the pair of quantum-particle conjugates time and energy and the two Fourier-wave-conjugates displacement and wave number become the pair of quantum-particle conjugates position and momentum.

The Heisenberg Uncertainty Principle dictates that a quantized electromagnetic oscillator (a.k.a. a photon state) can never come entirely to rest, since that would be a state of exactly zero energy, which is forbidden by the commutation relation given in the previous section. Instead, every mode of the field has $\hbar\omega/2$ as its average minimum energy in the vacuum, and this is called the zero-point energy (ZPE).^{**} This ZPE term is added to the classical blackbody spectral radiation energy density $\rho(\omega)d\omega$ [i.e., the energy per unit volume of radiation in the frequency interval $(\omega, \omega + d\omega)$] [25]:

^{**} $\hbar\omega$ is the energy of a single mode (or photon).

$$\begin{aligned}\rho(\omega) d\omega &= \frac{\omega^2}{\pi^2 c^3} \left[\frac{h\omega}{\exp(h\omega/k_B T) - 1} + \frac{h\omega}{2} \right] d\omega \\ &= \frac{h\omega^3}{2\pi^2 c^3} \coth\left(\frac{h\omega}{2k_B T}\right) d\omega,\end{aligned}\tag{2}$$

where k_B is Boltzmann's constant (1.3807×10^{-23} J/K) and T is the absolute temperature. The factor outside the square brackets in the first line of Eq. (2) is the density of mode (or photon) states (i.e., the number of states per unit frequency interval per unit volume); the first term inside the square brackets is the standard Planck blackbody radiation energy per mode; and the second term inside the square brackets is the quantum zero-point energy per mode. Equation (2) is called the Zero-Point Planck (ZPP) spectral radiation energy density. Planck first added the ZPE term to the classical blackbody spectral radiation energy density in 1912, although it was Einstein, Hopf, and Stern who actually recognized the physical significance of this term in 1913 [25]. Direct spectroscopic evidence for the reality of ZPE was provided by Mulliken's boron monoxide spectral band experiments in 1924, several months before Heisenberg first derived the ZPE for a harmonic oscillator from his new quantum matrix mechanics theory [39].

Following this line of reasoning, quantum physics predicts that all of space must be filled with quantum electromagnetic ZPF creating a universal sea of zero-point energy. The other quantum forces of nature also have their own vacuum ZPF which contributes to the universal sea of zero-point energy. But that is beyond the scope of this report.

Negative (Sub-Vacuum) Energy in Squeezed Light

Substantial theoretical and experimental work has shown that in many quantum systems the limits to measurement precision imposed by the quantum vacuum ZPF can be breached by decreasing the noise in one observable (or measurable quantity) at the expense of increasing the noise in the conjugate observable; at the same time the variations in the first observable, say the energy, are reduced below the ZPF such that the energy becomes "negative." "Squeezing" is thus the control of quantum fluctuations and corresponding uncertainties, whereby one can squeeze/reduce the variance of one (physically important) observable quantity provided the variance in the (physically unimportant) conjugate variable is stretched/increased. The squeezed quantity possesses an unusually low variance, meaning less variance than would be expected on the basis of the equipartition theorem. One can in principle exploit quantum squeezing to extract energy from one place in the ordinary vacuum at the expense of accumulating excess energy elsewhere [8].

The squeezed state of the electromagnetic field is a primary example of a quantum field that has negative energy density and negative energy flux. Such a state became a physical reality in the laboratory as a result of the nonlinear-optics technique of "squeezing," i.e., of moving some of the quantum-fluctuations of laser light out of the

$\cos[\omega(t - z/c)]$ part of the beam and into the $\sin[\omega(t - z/c)]$ part [18, 40-44].⁵⁵ The observable that gets squeezed will have its fluctuations reduced below the vacuum ZPF.

The act of squeezing transforms the phase space circular noise profile characteristic of the vacuum into an ellipse, whose semimajor and semiminor axes are given by unequal quadrature uncertainties (of the quantized electromagnetic oscillator operators). This applies to coherent states in general, and the usual vacuum is also a coherent state with eigenvalue zero. As this ellipse rotates about the origin with angular frequency ω , these unequal quadrature uncertainties manifest themselves in the electromagnetic field oscillator energy by periodic occurrences, which are separated by one quarter cycle, of both smaller and larger fluctuations compared to the unsqueezed vacuum.

We digress momentarily by noting that coherent states, also called Glauber states, are the eigenstates of the annihilation operator \hat{a} :

$$\hat{a}|\alpha\rangle = \alpha|\alpha\rangle, \quad (3)$$

which have well-defined amplitudes $|\alpha|$ and phases $\arg(\alpha)$ (recall the discussion in Sect. IIB-1). They are called coherent states because light fields in these states are perfectly coherent, and high-quality lasers generate such fields. This is an important reason why high-quality laser light is an excellent tool for experimental quantum optics. Coherent states come as close as quantum mechanics allows to wave-like states of the electromagnetic oscillator. Because the wave aspects of light are commonly regarded as classical, coherent states are often called classical states. Furthermore, fields in statistical mixtures of coherent states (such as thermal fields) are classical as well, whereas any state that cannot be understood as an ensemble of coherent states is called *nonclassical*. The experimental generation and application of nonclassical light fields is the main subject of this report. Despite much recent progress, producing nonclassical states of light is still extremely challenging because they are easily destroyed (reduced to classical) by any kind of losses. Furthermore, it turns out that the vacuum is a coherent state as well because it satisfies Eq. (3) for $\alpha = 0$. In other words, the vacuum is a zero-amplitude coherent state. With a little algebra we see directly from Eq. (3) that the mean (i.e., quantum expectation value of the) energy of a coherent state with unit frequency is

$$\begin{aligned} \langle \hat{H}_\alpha \rangle &= \langle \alpha | \hat{a}^\dagger \hat{a} + \frac{1}{2} | \alpha \rangle \\ &= |\alpha|^2 + \frac{1}{2}. \end{aligned} \quad (4)$$

Equation (4) is the sum of the classical wave intensity $|\alpha|^2$ and the vacuum zero-point energy $1/2$. One simply multiplies the right-hand side of Eq. (4) by $\hbar\omega$ to put $\langle \hat{H}_\alpha \rangle$ into units of energy.

⁵⁵ z denotes the z -axis direction of beam propagation.

Morris and Thorne [8] and Caves [45] point out that if one squeezes the vacuum, i.e., if one puts vacuum rather than laser light into the input port of a squeezing device, then one gets at the output an electromagnetic field with weaker fluctuations and thus less energy density than the vacuum at locations where $\cos^2[\omega(t-z/c)] \cong 1$ and

$\sin^2[\omega(t-z/c)] \ll 1$; but with greater fluctuations and thus greater energy density than the vacuum at locations where $\cos^2[\omega(t-z/c)] \ll 1$ and $\sin^2[\omega(t-z/c)] \cong 1$.

Since the vacuum is defined to have vanishing energy density, any region with less energy density than the vacuum actually has a negative (renormalized) expectation value for the energy density. Therefore, a squeezed vacuum state consists of a traveling electromagnetic wave that oscillates back and forth between negative energy density and positive energy density, but has positive time-averaged energy density.

In quantum optics the squeezed state is generated by the unitary squeezing operator:

$$\hat{S} \equiv \exp\left[\frac{\xi}{2}(\hat{a}^2 - \hat{a}^{\dagger 2})\right], \quad (5)$$

where ξ is a real number that parameterizes the deviation of the variances $\Delta\hat{q}$ and $\Delta\hat{p}$ from their vacuum values and is called the squeezing parameter. From Eq. (5) we obtain the *squeezed vacuum state* $|\varphi\rangle = \hat{S}(\xi)|0\rangle$. The squeezing operator $\hat{S}(\xi)$ is simply an evolution operator that describes the result of the nonlinear squeezing interaction Hamiltonian $\hat{H}_{\text{int}} = \chi(b^*\hat{a}^2 - b\hat{a}^{\dagger 2})$. The squeezing parameter ξ contains the product of the amplitude b , the coupling constant χ , and the interaction time.

But this is not the entire story. Since we will be dealing with high-quality lasers in what follows, we also need to know about another important quantum optics operator that acts on coherent states. We introduce the unitary displacement operator

$\hat{D}(\alpha) = \exp(\alpha\hat{a}^\dagger - \alpha^*\hat{a})$. $\hat{D}(\alpha)$ displaces the amplitude \hat{a} by the complex number α

according to $\hat{D}^\dagger(\alpha)\hat{a}\hat{D}(\alpha) = \hat{a} + \alpha$. To show why $\hat{D}(\alpha)$ has anything to do with coherent states, we apply a negative displacement to $|\alpha\rangle$. From the basic property of $\hat{D}(\alpha)$, we see that

$$\begin{aligned} \hat{a}\hat{D}(-\alpha)|\alpha\rangle &= \hat{D}(-\alpha)\hat{D}^\dagger(-\alpha)\hat{a}\hat{D}(-\alpha)|\alpha\rangle \\ &= \hat{D}(-\alpha)(\hat{a} - \alpha)|\alpha\rangle \\ &= 0. \end{aligned} \quad (6)$$

Equation (6) equals zero because of the definition Eq. (3) of coherent states. This result implies that $\hat{D}(-\alpha)|\alpha\rangle = |0\rangle$, which is the vacuum state. Therefore, coherent states $|\alpha\rangle$ are *displaced vacua* $|\alpha\rangle = \hat{D}(\alpha)|0\rangle$. This does not mean that coherent states

are physically similar to vacuum states, but instead they have only some quantum noise properties in common. It is a well known result in the quantum field theory of light that the vacuum wave function is a simple Gaussian function of the quadratures (in either \hat{q} or \hat{p} representation), and thus coherent states are also Gaussian [38]. Furthermore, a proof of Heisenberg's Uncertainty Principle in conjunction with the application of $\hat{S}(\xi)$ and $\hat{D}(\alpha)$ on the quadrature variances and wave functions showed that all minimum uncertainty states are displaced Gaussian states such that they have displaced rescaled vacuum wave functions. Consequently, all minimum uncertainty states are *displaced squeezed vacua* [18, 38]:

$$|\psi\rangle = \hat{D}(\alpha)\hat{S}(\xi)|0\rangle. \quad (7)$$

The squeezing interaction \hat{H}_{int} is realized by the degenerate parametric amplification of the spatial-temporal mode. A crystal such as potassium titanyl phosphate (KTP) or lithium niobate (LiNbO₃) is pumped by another laser beam with amplitude b and twice the frequency of the spatial-temporal mode (with amplitude \hat{a}) of interest. According to \hat{H}_{int} , the "B" photons (corresponding to b) of the pump beam are converted into pairs of "A" signal photons (corresponding to \hat{a}^2 and \hat{a}^{*2}) with a probability that depends on the coupling constant χ . The KTP or LiNbO₃ crystal acts like an electromagnetic swing, and the pump modulates the oscillation of the "A" mode at twice its frequency. The pump amplifies the signal parametrically much as a swing is amplified by changing the effective length at twice the frequency of the swing. A classical swing relies on tiny initial fluctuations (or "wobbles") that are in-phase with respect to the parametric pump. In this way, the tiny fluctuations are amplified; the swing starts to oscillate. A quantum swing like the degenerate parametric amplifier experiences at least the vacuum fluctuations from the very beginning. Vacuum fluctuations that are in-phase with respect to the pump are amplified, whereas out-of-phase fluctuations get de-amplified or, in other words, squeezed.

A squeezed vacuum requires a pump for generation, and, hence, when produced it carries energy. The nonlinear crystal KTP or LiNbO₃ is a resonator that is shaped like a cylinder with rounded silvered ends to reflect light. This resonator acts to produce a secondary lower frequency light beam in which the pattern of photons is rearranged into pairs. The squeezed light emerging from the resonator will contain pulses of negative energy interspersed with pulses of positive energy. To quantify the amount of squeezing energy we 1) apply $\hat{S}(\xi)$ to the quadratures and find that it scales their eigenfunctions;*** 2) we then substitute for \hat{a} its quadrature decomposition (given in Sect. IIB-1) and substitute that result into the scaled quadratures; and then 3) do further algebra to derive how $\hat{S}(\xi)$ changes \hat{a} : $\hat{S}^\dagger(\xi)\hat{a}\hat{S}(\xi) = \hat{a}\cosh\xi - \hat{a}^\dagger\sinh\xi$. We substitute this last result into Eq. (1) and use Eq. (7) to calculate the quantum expectation value in order to express the mean energy of a squeezed state, and obtain

*** i.e., \hat{q} gets squeezed and \hat{p} gets stretched.

$$\langle \psi | \hat{H}_{\text{sqvac}} | \psi \rangle = |\alpha|^2 + \frac{1}{2} + \sinh^2 \xi. \quad (8)$$

Equation (8) really describes the mean photon number of a single mode in a squeezed state, but one simply multiplies the right-hand side by $\hbar\omega$ to get the mean energy $\langle \hat{H}_{\text{sqvac}} \rangle = \hbar\omega \left(|\alpha|^2 + \frac{1}{2} + \sinh^2 \xi \right)$. We see in Eq. (8) that there are three terms contributing to the energy: the first term accounts for the coherent energy given by $|\alpha|^2$, the second term is the vacuum zero-point energy $1/2$, and the third term quantifies the fluctuation energy of squeezed states. The contribution to this squeezing energy originally comes from the pump used to generate the squeezed light. It is stored in the enhanced fluctuations of the anti-squeezed component. Because both the squeezed and the anti-squeezed quadratures contribute to the second line in Eq. (1), even a squeezed vacuum carries energy.

However, Eq. (8) is not the final result because it only gives the mean energy of a single mode in a squeezed state, while lasers and nonlinear crystal resonators produce a very large number of modes. Equation (8) needs to be summed (integrated) over the infinite number of possible modes; it must then be "renormalized" by sophisticated mathematical techniques in order to get rid of the divergent (infinite) contribution from the vacuum zero-point energy (a byproduct of taking an infinite sum of modes); and then the result must be converted into units of energy density by dividing it by an appropriate volume element, because Einstein's general theory of relativity requires an energy density (or pressure, both are in the same units) to induce spacetime bending. The final result we seek is the energy density, $\rho_{\text{E-sqvac}}$, given by Pfenning [46]:

$$\rho_{\text{E-sqvac}} = \left(\frac{2\hbar\omega}{L^3} \right) \sinh \xi \left[\sinh \xi + \cosh \xi \cos(2\omega(t - z/c) + \delta) \right] \quad (\text{J/m}^3), \quad (9)$$

where L^3 is the volume of a large box with sides of length L (i.e., we put the quantum field in a box with periodic boundary conditions) and δ is the phase of squeezing. Equation (9) shows that $\rho_{\text{E-sqvac}}$ falls below zero once every cycle when the condition $\cosh \xi > \sinh \xi$ is met. It turns out that this is always true for every nonzero value of ξ , so $\rho_{\text{E-sqvac}}$ becomes negative at some point in the cycle for a general squeezed vacuum state. See Figure 1 for an illustration. Note in the figure that the blue troughs or valleys are the negative energy pulses. On another note, when a quantum state is close to a squeezed vacuum state, there will almost always be some negative energy densities present.

Another way to generate negative energy via squeezed light would be to manufacture extremely reliable light pulses containing precisely one, two, three, etc., photons apiece and combine them together to create squeezed states to order. Superimposing many such states could theoretically produce bursts of intense negative energy. Photonic crystal research has already demonstrated the feasibility of using photonic crystal waveguides (mixing together the classical and quantum properties of optical materials) to engineer light sources that produce beams containing precisely one, two, three, etc., photons. See Reference [1] for more details and for the references cited therein.

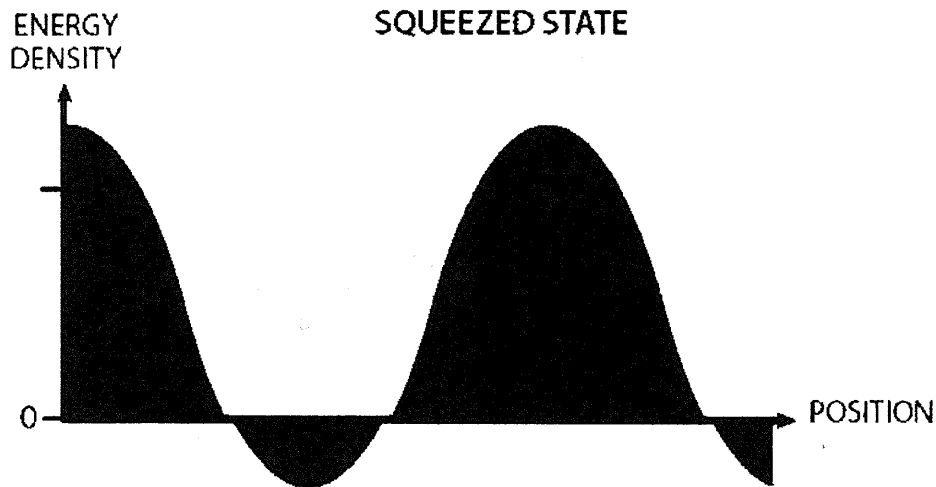


Figure 1. Illustration of a Squeezed State of Light. (courtesy of Lisa Burnett)

Negative (Sub-Vacuum) Energy in the Casimir Effect

The Casimir effect originates from the quantum electromagnetic vacuum ZPF. It is by far the easiest and most well known way to generate (static) negative energy in the lab. The Casimir effect that is familiar to most people is the force that is associated with the quantum vacuum electromagnetic ZPF [47]. This is an attractive force that must exist between any two neutral (uncharged), parallel, flat, conducting surfaces (e.g., metallic plates) in a vacuum. This force has been well measured and it can be attributed to a minute imbalance in the vacuum electromagnetic ZPE density inside the cavity between the conducting surfaces versus the vacuum electromagnetic ZPE density in the free-space region outside of the cavity [48-50]. See Figure 2 for a schematic of the Casimir effect.

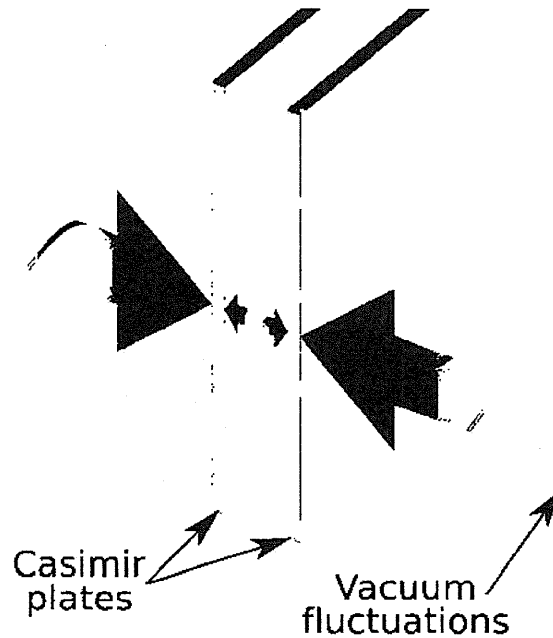


Figure 2. Schematic of the Casimir Effect.

It turns out that there are many different types of Casimir effects found in quantum field theory [20-22, 26-28, 51]. For example, if one introduces a single infinite plane conductor into the Minkowski (flat spacetime) vacuum by bringing it adiabatically from infinity so that whatever quantum fields are present suffer no excitation but remain in their ground states, then the vacuum (electromagnetic) stresses induced by the presence of the infinite plane conductor produces a Casimir effect. This result holds equally well when two parallel plane conductors (with separation distance d) are present, which gives rise to the familiar Casimir effect inside a cavity. Note that in both cases, the spacetime manifold is made incomplete by the introduction of the plane conductor boundary condition(s). The vacuum region put under stress by the presence of the plane conductor(s) is called the Casimir vacuum. The generic expression for the energy density of the Casimir effect is $\rho_{CE} = -A\hbar cd^{-4}$, where $A = \zeta(D)/8\pi^2$ in spacetimes of arbitrary dimension D [20-22]. The appearance of the zeta-function $\zeta(D)$ is characteristic of expressions for vacuum stress-energy tensors, $T_{vac}^{\mu\nu}$.^{††} In our familiar 4-dimensional spacetime ($D = 4$) we have that $A = \pi^2/720$. To calculate $T_{vac}^{\mu\nu}$ for a given quantum field is to calculate its associated Casimir effect.

We should also point out that the methods used to obtain the quantum vacuum electromagnetic $T_{vac}^{\mu\nu}$ between parallel plane conductors can also be used when the conductors are not parallel but are joined together along a line of intersection. If the conductors have curved surfaces instead, then one obtains results that are similar to the case of intersecting conductors. These geometries have also been evaluated for the

^{††} The Greek tensor indices ($\mu, \nu = 0...3$) denote spacetime coordinates, $x^0...x^3$, such that $x^1...x^3 \equiv$ space coordinates and $x^0 \equiv$ time coordinate. Note in general that $T^{00} \equiv \rho_E$ (field energy density).

case of dielectric media. These particular cases will not be considered further since there are technical subtleties involved that complicate the calculations and application of the different approaches.

As a final note, negative energy can be created by a single moving reflecting (conducting) surface (a.k.a. a moving mirror) via the dynamical Casimir effect. A mirror moving with increasing acceleration generates a flux of negative energy that emanates from its surface and flows out into the space ahead of the mirror [23, 52]. This is essentially the simple case of an infinite plane conductor undergoing acceleration perpendicular to its surface. If the acceleration varies with time, the conductor will generally emit or absorb photons (i.e., exchange energy with the vacuum), even though it is neutral. This is an example of the well-known quantum phenomenon of parametric excitation. The parameters of the quantum electromagnetic oscillators (e.g., their frequency distribution function) change with time owing to the acceleration of the mirror [53]. However, this effect is known to be exceedingly small, and it is not the most effective way to produce negative energy for our purposes. We will not consider this scheme any further.

QUANTUM OPTICAL HOMODYNE TOMOGRAPHY

Observing Negative Energy in the Lab

Negative energy should be observable in lab experiments. A generic, non-optical scheme for detecting negative energy in experiments was recently reported by Davies and Ottewill [54] who studied the response of switched particle detectors to static negative energy densities and negative energy fluxes. Their model is based on a free (massless) scalar field in flat 4-dimensional Minkowski spacetime and utilized a simple generalization of the standard monopole detector, which is switched on and off to concentrate the measurements on periods of isolated negative energy density (or negative energy flux). The detector model includes an explicit switching factor whereby five different switching functions (based on data windowing theory) are defined and evaluated.

In order to isolate the effects of negative energy, a comparison is made for the response of a detector switched on and off during a period of negative energy density (or negative energy flux) and that switched on and off in the vacuum. The results shed light on the response of matter (detectors) to pulses of negative energy of finite duration, and they showed that negative energy should have the effect of enhancing de-excitation (i.e., induce cooling) of the detector. This is the opposite of our experience with detectors that undergo excitation when encountering "normal" matter or energy, and isolated detectors placed in a vacuum naturally cool due to the usual thermodynamic reasons. But Davies and Ottewill point out that the enhanced cooling effect they discovered cannot be used to draw a thermodynamic conclusion because their modeling was restricted to first order in perturbation theory. It is not possible at first order to determine whether the enhanced cooling effects are due to the small violation of energy conservation expected in any process in which a general quantum state collapses to an energy eigenstate, or whether they predict a systematic reduction in the energy of the detector which has serious thermodynamic implications. However, Davies and Ottewill point out that their results are model dependent and they found for their standard monopole detector model that there is not always a simple relationship

between the strength of the negative energy density/flux and the behavior of the detector.

It is curious that Davies and Ottewill did not consider using quantum optical homodyne tomography as a tool to test their hypothesis, because this is already a mature experimental discipline. In what follows we outline the basics of quantum optical homodyne tomography and its application to detecting and measuring negative energy density/flux states in squeezed light and in the Casimir effect.

Basic Notions of Quantum Optical Homodyne Tomography

Tomography, from the Greek word for *slice*, is a method to infer the shape of a hidden object from its shadows (or projections) under various angles. Quantum tomography is the application of this idea to quantum mechanics. In optical homodyne tomography, the Wigner function or, more generally, the quantum state plays the role of the hidden object. The observable "quantum shadows" are the quadrature distributions and are measured using homodyne detection. From these distributions the Wigner function is reconstructed. See Figure 3 for an illustration of quantum optical homodyne tomography. The vertical 2-dimensional plane seen in the figure is fictitious and is shown for illustrative purposes only.

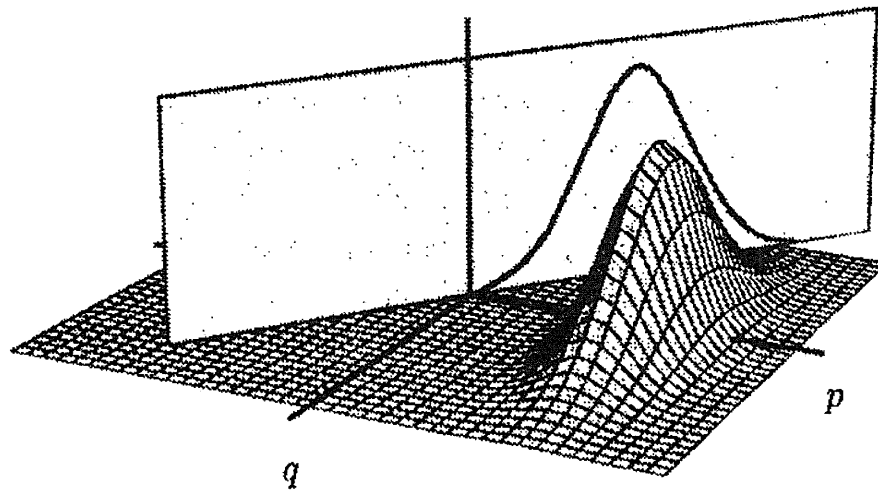


Figure 3. Illustration of Quantum Optical Homodyne Tomography (courtesy of Ulf Leonhardt). The Wigner function (3-dimensional hill on the right) is reconstructed in quantum phase space (gridded plane formed by quadratures q and p) from its experimentally measured projections (curve in vertical 2-dimensional plane), which represents the scanning process of tomography. The vertical axis is the magnitude of the Wigner (quasiprobability) function.

Quantum tomography was developed for the simple reason that a fundamental feature of quantum mechanics prevents us from seeing physical objects in their full quantum complexity. This is due to the intrinsic fuzziness in the quantum nature of energy and matter according to the Heisenberg Uncertainty Principle, which prevents us from simultaneously and precisely measuring the complementary features (e.g., position and momentum or energy and time) comprising quantum states. For this reason we cannot

directly observe quantum states, and so the true nature of an individual quantum system is hidden. However, no principal obstacle exists to observing all complementary aspects in a series of distinct experiments on identically prepared quantum objects.

In the sections that follow, we briefly review the several parts that comprise the tomography machinery, and then put the whole picture together to understand what the entire process is. No effort will be made for completeness because the subject of quantum tomography takes up volumes of books. The reader will be referred to the key literature of importance.

Wigner Functions

In classical optics the state of an electromagnetic oscillator is perfectly described by the statistics of the classical amplitude α . The amplitude may be completely fixed (then the field is coherent), or α may fluctuate (then the field is partially coherent or incoherent). In classical optics as well as in classical mechanics, we can characterize the statistics of the complex amplitude α or, equivalently, the statistics of the component position q and momentum p by introducing a phase space distribution called the Wigner function, $W(q,p)$.^{***} $W(q,p)$ quantifies the probability of finding a particular pair of q and p values in their simultaneous measurement. Knowing $W(q,p)$ for a particular quantum state that is under study, all statistical quantities of the electromagnetic oscillator can be predicted by calculation. In this sense $W(q,p)$ describes the state in classical physics. The motivation for introducing the Wigner function was the desire to find a quantum mechanical description similar to that in classical statistical physics. However, in quantum mechanics Heisenberg's Uncertainty Principle prevents one from observing position and momentum simultaneously and precisely. In addition to this, we also cannot directly observe quantum states either. Nevertheless, we are perfectly entitled to use the concept of quantum states as if they were existing entities. We use their properties to predict the statistics of observations.

It is well known that the quantum mechanical wave function depends exclusively on either the position or the momentum and contains nevertheless *all* the information about the quantum system under study. However, E. Wigner showed that it is possible to define a formal quantum mechanical analog to the classical distribution function. He showed that we could use $W(q,p)$ as a quantum phase space distribution exclusively to calculate observables in a classical-like fashion. Wigner discovered that $W(q,p)$ is a real-valued function, but it is usually not just positive; it can also become negative. This is a very nonclassical behavior for a probability distribution. It is for this reason that $W(q,p)$ came to be called a *quasiprobability* distribution.

$W(q,p)$ has several properties and mathematical postulates, but it turns out that just one postulate is sufficient for the purposes of quantum tomography [38]. Using this postulate, it is assumed that $W(q,p)$ behaves like a joint probability distribution for q and p without ever mentioning any simultaneous observation of position and momentum. The reduced, or *marginal*, distributions $\int_x^{-x} W(q,p) dp$ or $\int_x^{+x} W(q,p) dq$

^{***} Recall in Sect. IIB-1 that the real and the imaginary parts of the complex amplitude α can be regarded as the position and the momentum of the electromagnetic oscillator.

must give the position or the momentum distribution, respectively. Furthermore, if one performs a phase shift θ all complex amplitudes \hat{a} are shifted in phase,⁵⁶⁵ meaning that the components q and p rotate in the 2-dimensional phase space (q,p) . A classical probability distribution for position and momentum values would rotate accordingly. This fact leads to the postulate that the position probability distribution $pr(q,0)$ after an arbitrary phase shift θ should be [38]

$$\begin{aligned} pr(q,\theta) &\equiv \langle q | \hat{U}(\theta) \hat{\rho} \hat{U}^\dagger(\theta) | q \rangle \\ &= \int_{-\infty}^{\infty} W(q \cos \theta - p \sin \theta, q \sin \theta + p \cos \theta) dp, \end{aligned} \quad (10)$$

where $\hat{\rho}$ is the quantum density operator (or density matrix) which describes the statistical (or most general) state of a quantum system. The first line in Eq. (10) is the quantum expectation value of the phase-shifted $\hat{\rho}$, which simply gives the probability distribution for the q -eigenstates to occur with probabilities ρ_q (the elements of $\hat{\rho}$). This single formula joins $W(q,p)$ with quantum mechanics. It ties $W(q,p)$ to observable quantities, and it links quantum states to observations.

It is beyond the scope of this report to repeat the entire mathematical development of the explicit functional representations, identities, transformations and modifications of $W(q,p)$. The reader should consult Reference [38] for more information. However, Figures 4 through 7 provide an example of what the experimentally reconstructed Wigner function visually looks like from the quantum optical homodyne tomography of the following cases of interest: a vacuum state, a coherent state, a squeezed vacuum state, a single photon, and Schrödinger cat states. The Schrödinger cat states are a very interesting case study of unusual nonclassical states of light that have been experimentally measured via quantum optical homodyne tomography.

⁵⁶⁵ The unitary phase shifting operator is $\hat{U}(\theta) = \exp(-i\theta\hat{n})$, where \hat{n} is the photon number operator and θ is the phase shift angle. Its action on the amplitude \hat{a} is: $\hat{U}^\dagger(\theta)\hat{a}\hat{U}(\theta) = \hat{a}\exp(-i\theta)$.

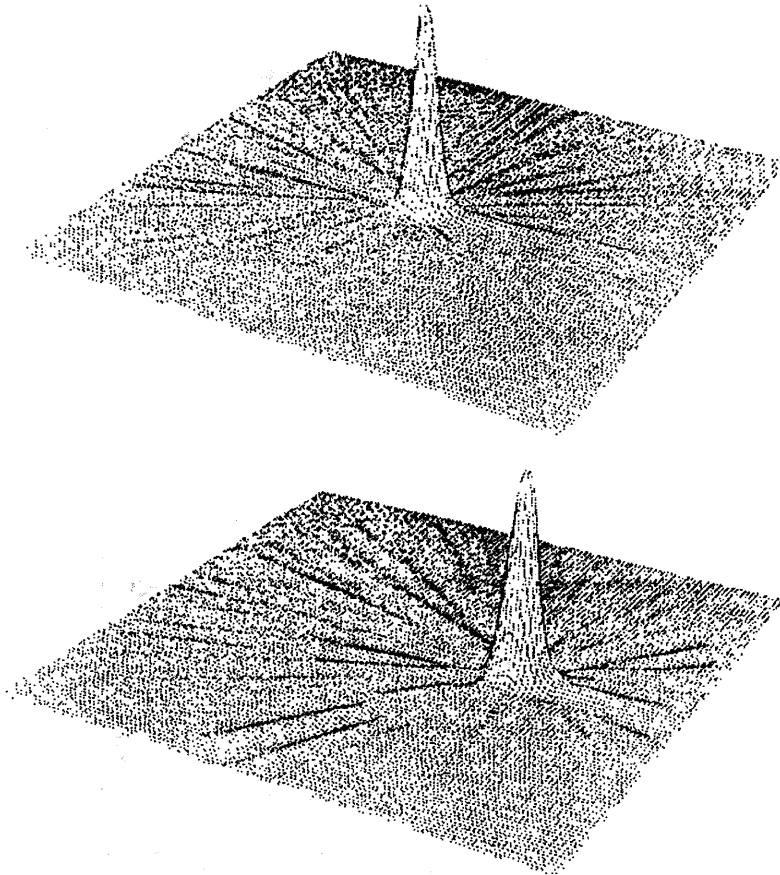


Figure 4. Wigner Function for a Vacuum (top) and for a Coherent State (bottom). This clearly shows that coherent states are just "displaced vacua" (Sect. IIB-3). Optical homodyne tomography was used to reconstruct the Wigner functions from experimental data (courtesy of Ulf Leonhardt).

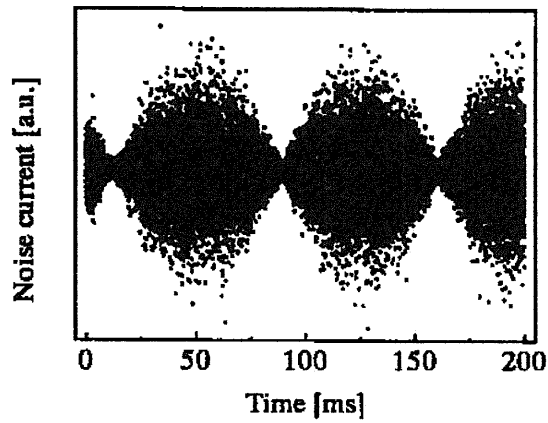
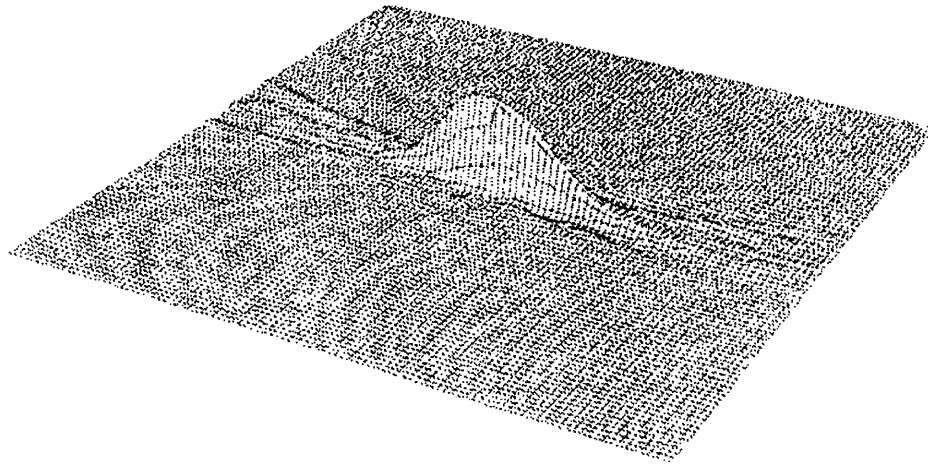


Figure 5. Wigner Function of a Squeezed Vacuum. Wigner function (top) and quadrature fluctuations (bottom). This shows the experimentally reconstructed Wigner function of a significantly squeezed vacuum generated by parametric amplification (Sect. IIB-3). The noise trace (bottom) shows a part of the experimental data used to reconstruct the depicted Wigner function via optical homodyne tomography (courtesy of Ulf Leonhardt).

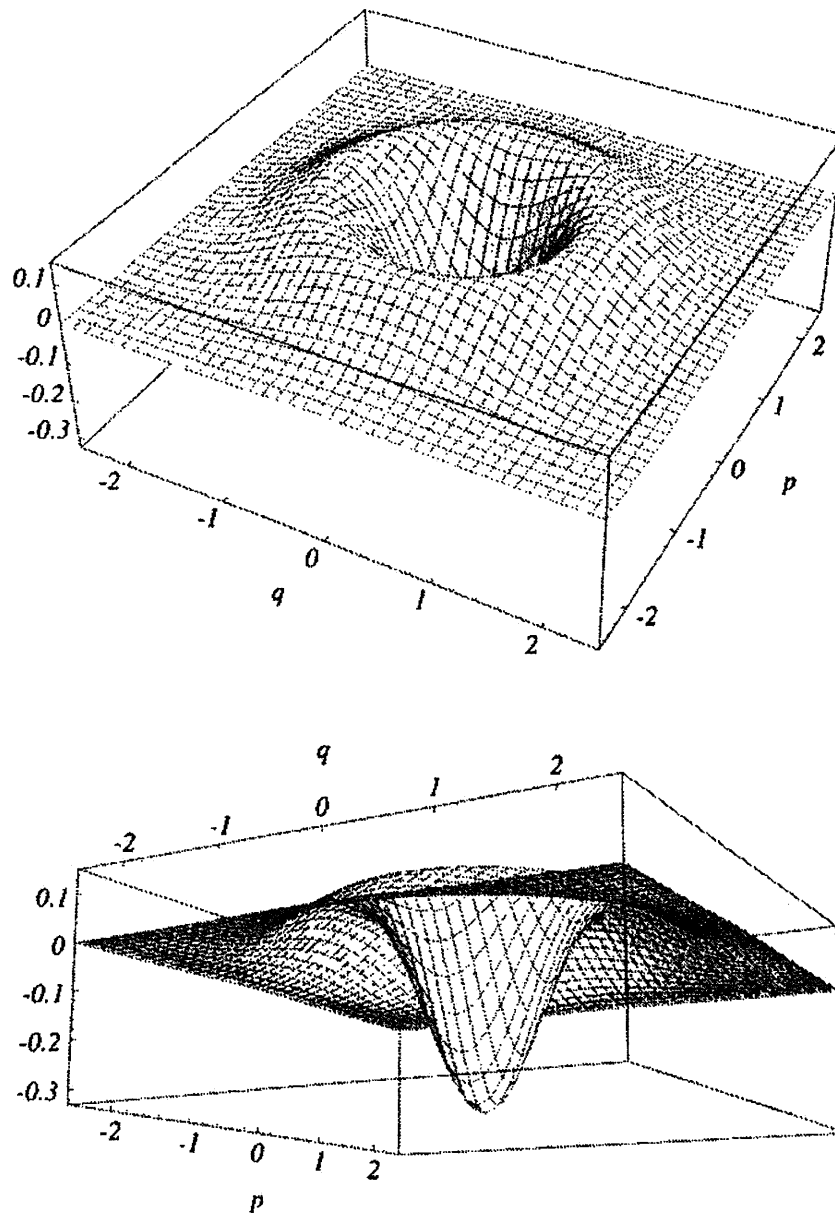


Figure 6. Wigner Function of a Single Photon. The figure shows the experimentally reconstructed Wigner function as seen from above (top) and from below (bottom). Negative "probabilities" are clearly visible near the origin of the phase space, which demonstrates the nonclassical aspect of photons (courtesy of Ulf Leonhardt).

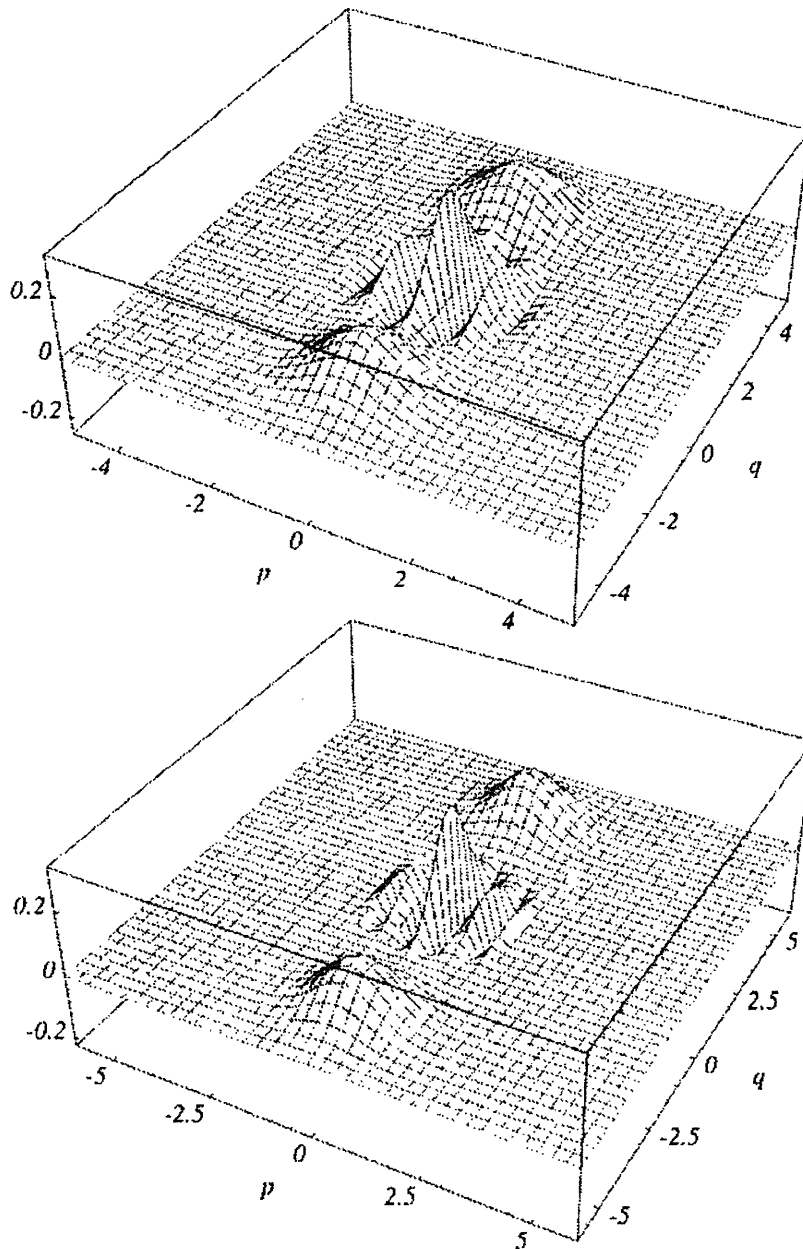


Figure 7. Quantum Tomography of Schrödinger-Cat States. Top: $q_0 = 3$. Two separated coherent amplitudes (peaks) are clearly visible. Bottom: $q_0 = 4$. The larger the separation of the amplitudes, the more rapid is the oscillation in the quantum interference structure between the two peaks. Negative probabilities appear within the quantum interference structure. The experimental data used to reconstruct the depicted Wigner functions was provided by A. Furusawa and H. Yonezawa, University of Tokyo.

We digress for the moment to explain what Schrödinger cat states are. Schrödinger's cat is a famous illustration of the principle of superposition in quantum theory that was proposed as a thought experiment by Erwin Schrödinger in 1935. Schrödinger's cat

serves to demonstrate the apparent conflict of what quantum theory tells us is true about the nature and behavior of matter on the quantum (atomic or subatomic) level compared with what we actually observe to be true about the nature and behavior of matter on the macroscopic level.

Schrödinger's thought experiment is as follows: One places a living cat into a steel chamber along with a device containing a vial of hydrocyanic acid. There is also a very small amount of a radioactive substance inside the chamber. If even a single atom of the substance decays during the test period, then a relay mechanism will trip a hammer, which will in turn break the vial and kill the cat.

The observer cannot know whether or not an atom of the radioactive substance has decayed, and consequently, cannot know whether the vial has been broken, the hydrocyanic acid released, and the cat killed. Since one cannot know, the cat is both dead and alive in a superposition of quantum states according to the quantum superposition principle. It is only when one breaks open the box and learns the condition of the cat that the superposition is lost, and the cat becomes either dead or alive. This situation is sometimes called *quantum indeterminacy* or *the observer's paradox*: the act of observation or measurement itself affects the outcome, so that the outcome as such does not exist unless, and until, the measurement is made. (That is, there is no single outcome unless it is observed.)

According to the fundamental superposition principle of quantum mechanics, we are entitled to think of quantum superpositions of coherent states. These are states that contain simultaneously two coherent components (or states), one pointing in one direction in phase space and the other pointing in another direction. We label the former component the "alive-cat" state and the latter component the "dead-cat state." The position wave function Ψ of such a state would be the superposition of two coherent state (Gaussian) wave functions [38]:

$$\Psi(q) \propto \exp\left[-\frac{1}{2}(q-q_0)^2\right] + \exp\left[-\frac{1}{2}(q+q_0)^2\right]. \quad (11)$$

The normalization factor has been omitted in Eq. (11) because it is not important here. Equation (11) shows that Ψ has two peaks, one at $+q_0$ (alive-cat state) and the other at $-q_0$ (dead-cat state) according to the superimposed coherent amplitudes. Also, Eq. (11) has nothing to do with optical interference. When two fields interfere, their amplitude may be enhanced or canceled, producing, for example, coherent states of enhanced or zero amplitude (vacuum). The quantum superposition shown in Eq. (11) still contains both coherent amplitudes $\pm q_0$. It is also much different from an incoherent superposition of $\pm q_0$, where the field has either the amplitude $+q_0$ or the amplitude $-q_0$ with certain probabilities. The quadrature amplitude of Ψ is $+q_0$ as well as $-q_0$ (*simultaneously!*), with a resolution given by the vacuum fluctuations.

This strange behavior of Ψ being simultaneously at $+q_0$ and $-q_0$ turns out to be the best representation of Schrödinger's famous thought experiment in the quantum field theory of light. Schrödinger cat states are difficult to observe in the optical domain because

they are extremely vulnerable to quantum decoherence. Quantum decoherence is caused by linear losses, and it is the main reason why the extremely strange quantum phenomena allowed in quantum theory are very difficult to observe in practice. However, the good news is that investigators have successfully controlled or suppressed quantum decoherence to such a high degree that Schrödinger cat states were experimentally observed and measured using optical homodyne tomography [55, 56]. Figure 7 shows the experimentally reconstructed Wigner functions for two Schrödinger cat states that have different amplitude values $\pm q_0$. The observed peaks at $\pm q_0$ seen in the figure are of small magnitude, so investigators euphemistically call these "Schrödinger kitten states." As seen in the figure, the interference structure halfway between the peaks displays the quantum superposition of both amplitudes, showing rapid oscillations with a frequency given by the distance $2|q_0|$ of the superimposed amplitudes. Also seen in the figure is that the two reconstructed Wigner functions become negative (i.e., negative "probabilities"), indicating the nonclassical behavior of Schrödinger cat/kitten states.

Beam Splitters

A very important device that is used to demonstrate the quantum nature of light is the simple optical beam splitter. A large number of strange quantum effects have been experimentally observed by splitting or recombining photons using a small cube of glass. The beam splitter also serves as a theoretical model for other linear optical devices such as interferometers, semitransparent mirrors, dielectric interfaces, waveguide couplers, and polarizers. The beam splitter model can also be used to account for the effect of absorption, mode mismatch, and other linear losses.

An ideal beam splitter is a reversible, lossless device in which two incident beams of light may interfere to produce two emerging beams [38]. For example, a dielectric interface inside a cube or plate of glass splits a light beam into two. This situation may be reversed by sending the two beams back to the cube (or plate) where they interfere constructively to restore the original beam. However, if the phases of the two beams are changed, then their mutual interference generates two emerging beams in general. So four beams might be involved, two incident light modes and two outgoing light modes, and the splitting of just one beam is a special case. Therefore, the most general theoretical beam splitter model is a *four-port* device, which is simply a "black box" with two input and two output ports having certain mathematical and physical properties [38]. See Figure 8 for a schematic of an ideal lossless four-port beam splitter.

The beam splitter is quantum mechanically described by a simple unitary transformation operator (or matrix), based on an analog transformation matrix in classical optics,^{****} which mathematically transforms the two input light modes into the two output light modes. This operator is unitary, which reflects the fact that a lossless beam splitter conserves energy and that the total light mode intensity $\hat{a}_1^\dagger \hat{a}_1 + \hat{a}_2^\dagger \hat{a}_2$ is an invariant quantity. Since the incoming and the outgoing light modes are both independent bosonic modes, their annihilation operators must satisfy the following

^{****} In classical optics, the components of the transformation matrix of a real beam splitter are simply the transmissivity and reflectivity, which account for the transmission and reflection probabilities of photons passing through the glass cube or plate.

bosonic commutation relations: $[\hat{a}'_l, \hat{a}'_m{}^\dagger] = [\hat{a}_l, \hat{a}_m{}^\dagger] = \delta_{lm}$ and $[\hat{a}'_l, \hat{a}'_m] = [\hat{a}_l, \hat{a}_m] = 0$, where δ_{lm} ($= 1$ if $l = m$ and 0 if $l \neq m$) is the Kronecker delta and the indices (l, m) are integers [38].

A beam splitter is a four-port device not only in the case of two incoming light modes interfering to produce two emerging light modes; a beam splitter is always a four-port device. Even if only one beam is split into two beams, if literally nothing behind the semitransparent mirror is interfering with the incident beam, quantum mechanically *this nothing means a vacuum state*. The very possibility that the second light mode behind the mirror might be excited makes a difference. The vacuum fluctuations carried by the empty mode (and entering the apparatus via the so-called unused input port of the beam splitter) do cause physical effects. Therefore, the vacuum fluctuations entering the second (unused) input port of the beam splitter must always be assigned a formal mode operator, \hat{a}_2 , in order for the system to 1) conserve energy, 2) obey the beam splitter's aforementioned bosonic commutation relations and 3) guarantee that the two outgoing beams are independent bosonic light modes.

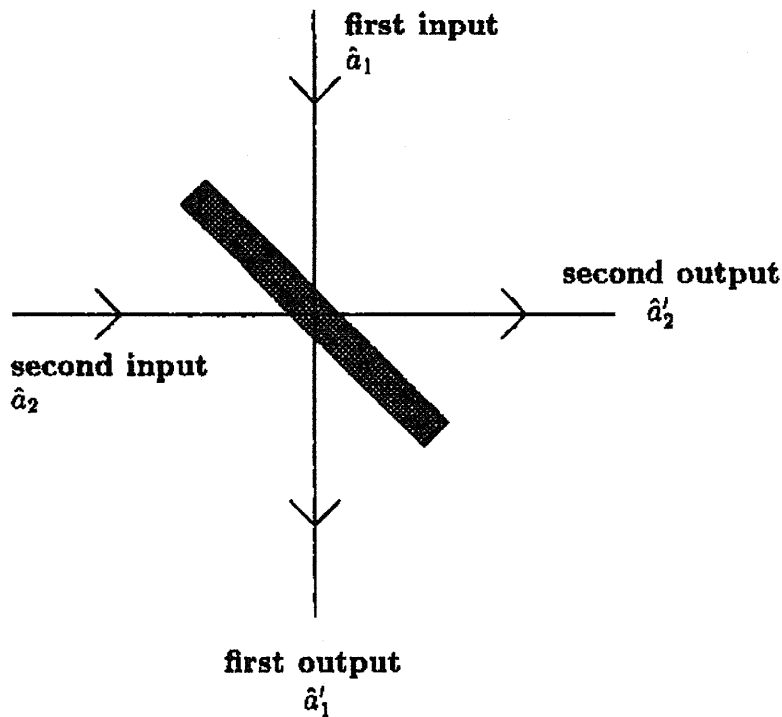


Figure 8. Schematic of an Ideal Lossless Beam Splitter. Two incident spatial-temporal light modes (with the annihilation operators \hat{a}_1 and \hat{a}_2) interfere optically to produce two emerging light modes (with the annihilation operators \hat{a}'_1 and \hat{a}'_2) (courtesy of Ulf Leonhardt).

In Figure 9 we illustrate the effect of vacuum fluctuations for the case of a fictitious beam splitter, which is a model for describing linear absorption or, equivalently,

detection losses. The input signal \hat{a} is attenuated and, simultaneously, contaminated by the vacuum fluctuations entering the second (unused) input port of the fictitious beam splitter. The absorber acts like a fictitious beam splitter, and when light is attenuated it can be imagined as being split into a transmitted part and an absorbed part. On the other hand, we know from the fluctuation-dissipation theorem that losses are always accompanied by fluctuations [57]. At least the vacuum fluctuations of the absorbing medium must be taken into account. In the simple absorber model, these fluctuations come into play via the second (unused) input port of the fictitious beam splitter as shown in Figure 9. The annihilation operator \hat{a} of the partially absorbed (input signal) mode is transformed by the fictitious beam splitter according to $\hat{a}' = \eta^{1/2}\hat{a} + (1-\eta)^{1/2}\hat{a}_2$, where the factor η ($0 < \eta \leq 1$) reduces the intensity of any initial coherent state $|\alpha\rangle$ to $|\eta^{1/2}\alpha\rangle$ after undergoing partial absorption, \hat{a}' is the output signal mode that goes to the detector (which counts the number of photons it absorbs, $\hat{n}' \equiv \hat{a}'^\dagger \hat{a}'$), and \hat{a}_2 is the mode operator of the vacuum fluctuations entering the second (unused) input port of the fictitious beam splitter. The second term $(1-\eta)^{1/2}\hat{a}_2$ in \hat{a}' is essential to guarantee that the attenuated light field remains a proper bosonic mode, otherwise energy conservation and the aforementioned bosonic commutation relations would be violated.

Finally, we note without further elaboration that the mode operators, quadrature wave functions, and Wigner functions are all rotated through some angle under the action of a beam splitter. And the Wigner function of a signal is smoothed during absorption under the action of a fictitious beam splitter. This provides additional models to develop the properties of other types of optical instruments and understand their behavior on incoming light modes (or input signals).

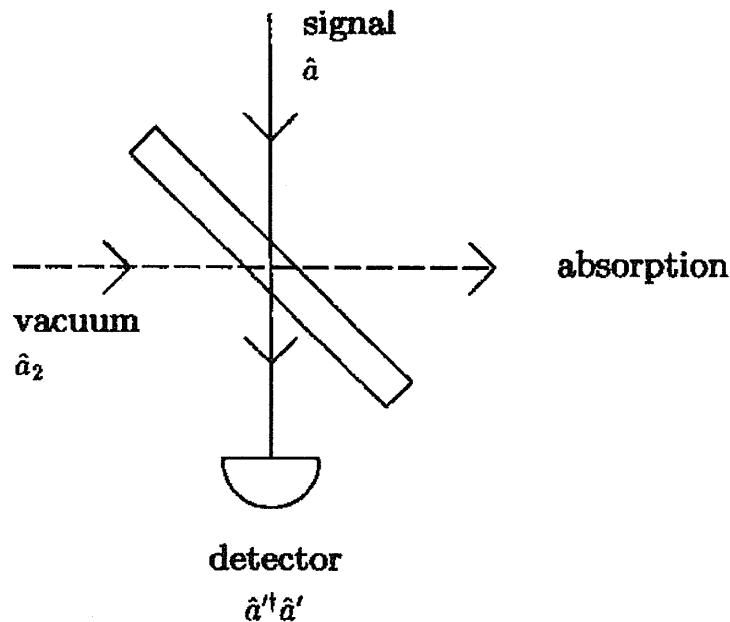


Figure 9. Illustration of a Fictitious Beam Splitter.
(courtesy of Ulf Leonhardt)

Photodiodes

Most photodetectors apply a version of the photoelectric effect to operate in which incident light radiation ionizes a piece of photosensitive material in the detector and produces freely moving electrons, i.e., an electric current is created that can be amplified and handled by electronic means. A commonly used type of detector is the linear-response photodiode. In most cases, the photosensitive part of the detector is a *P-I-N* structure, a sandwich of *Positively* doped, *Intrinsic*, and *Negatively* doped semiconductor material. Commonly, silicon (Si) or indium gallium arsenide (InGaAs) are used where Si detects light out to a 1 μm wavelength and InGaAs operates in the range 0.19 μm to 2.6 μm . A bias voltage of about 10 Volts is applied to drain the majority carriers (electrons in *N* and holes in *P*) out of the intrinsic zone. In this depletion region an unstable situation is created for the minority carriers. As soon as electron-hole pairs are present in the intrinsic zone, the bias voltage produces a current that is proportional to the number of carriers. Electrons in the valence band are lifted into the conduction band by the absorption of light radiation, i.e., the absorption of a single photon lifts one electron into the conduction band, which creates electron-hole pairs in the depletion zone. This process can be made highly efficient because the applied voltage is very low so that no avalanche of charge carriers into the conduction band (via collisions) is formed. The current response of the detector is linear in the intensity of the detected light. However, thermal fluctuations cause Nyquist noise in the photocurrent. Thermal effects also create electron-hole pairs in the depletion zone thus producing dark current, which is electronic noise. Because of this electronic noise, linear-response photodiodes do not reach single-photon resolution. They are suitable for relatively high intensities, greater than about 100 photons per microsecond.

There are inefficiencies and noise associated with realistic photodetection. A convenient model to understand the effect these have on experiments is provided by imagining a fictitious beam splitter placed in front of an ideal detector. See Figure 9. Only the transmitted photons are counted, so that the transmissivity of the fictitious beam splitter corresponds to the detection efficiency. Dissipation is always accompanied by fluctuations. These degrade the quantum noise properties of the detected light. The fluctuations are modeled by a vacuum entering the unused port of the fictitious beam splitter. This analysis shows how the nonclassical features of light are lost when the detectors are inefficient.

Balanced Homodyne Detection

Under idealized conditions the photon number is measured in direct photodetection. However, another method of detection exists, in which the light field amplitudes (the quadrature components) are measured instead of the quantized light intensity. Intensity (photon number) and field amplitude (quadrature) are distinct quantities. There is no simple relationship between the photon statistics and the quadrature distributions in the quantum regime, but the two are shown to be related via the mathematics and procedures of quantum state sampling [38]. Furthermore, the field amplitudes contain phase information, and so they are dependent on phase.

Quadrature components \hat{q}_0 are defined^{***} with respect to a certain reference phase θ that can be varied experimentally.

The principle scheme of a balanced homodyne detector is depicted in Figure 10. The signal interferes with a coherent laser beam at a well-balanced 50:50 beam splitter. The laser light field is called the *local oscillator* (LO), and it provides the phase reference θ for the quadrature measurement. It is assumed that the signal and the LO have a fixed phase relation, as is the case in most experiments applying homodyne detection, because both fields are ultimately generated by a common master laser. The LO should be intense with respect to the signal for providing a precise phase reference. It is also assumed that the LO is powerful enough to be treated classically, i.e., we totally neglect the quantum fluctuations of the LO. After the optical mixing of the signal with the LO, each emerging beam is directed to a linear-response photodiode. The photocurrents I_1 and I_2 are measured, electronically processed, and finally subtracted from each other. The difference current $I_{21} \equiv I_2 - I_1$ is the quantity of interest because it contains the interference term of the LO and the signal. It is assumed for simplicity that the measured photocurrents I_1 and I_2 are proportional to the photon numbers \hat{n}_1 and \hat{n}_2 of the beams striking each detector, which are given by $\hat{n}_1 = \hat{a}'_1 \hat{a}'_1$ and $\hat{n}_2 = \hat{a}'_2 \hat{a}'_2$ in terms of the mode operators $\hat{a}'_1 = 2^{-1/2}(\hat{a} - \alpha_{LO})$ and $\hat{a}'_2 = 2^{-1/2}(\hat{a} + \alpha_{LO})$ of the fields emerging from the beam splitter [38]. Here \hat{a} denotes the annihilation operator of the signal and α_{LO} is the complex amplitude of the LO.

The difference current I_{21} is proportional to the difference photon number (assuming perfect quantum efficiency) $\hat{n}_{21} = \hat{n}_2 - \hat{n}_1 = \alpha_{LO}^* \hat{a} + \alpha_{LO} \hat{a}^\dagger$, where α_{LO}^* is the complex conjugate of α_{LO} . The phase of the LO is θ , and so we note from the definition of \hat{q}_θ that the measured quantity I_{21} is indeed proportional to \hat{q}_0 because $\hat{n}_{21} = 2^{1/2} |\alpha_{LO}| \hat{q}_0$, which is a result that has been verified by more sophisticated theories of homodyne detection [38]. A balanced homodyne detector measures \hat{q}_0 . The reference phase θ is provided by the LO and can be varied by adjusting the LO using a piezo-electrically movable mirror, for example. An experimental method for finding the scaling of \hat{q}_0 in the difference current I_{21} is to keep a record of the sum current because the sum of I_1 and I_2 is proportional to $|\alpha_{LO}|^2$ to leading order [38]. This can be experimentally important because the intensity of the LO is usually an unknown quantity.

*** We note that phase shifting rotates the quadratures, $\hat{q}_0 \equiv \hat{U}^\dagger(\theta) \hat{q} \hat{U}(\theta) = \hat{q} \cos\theta + \hat{p} \sin\theta$ and $\hat{p}_0 \equiv \hat{U}^\dagger(\theta) \hat{p} \hat{U}(\theta) = -\hat{q} \sin\theta + \hat{p} \cos\theta$, via the quadrature decomposition defined in Sect. IIB-1 and the phase shifting property of the annihilation operator defined in Sect. IIIB-1.

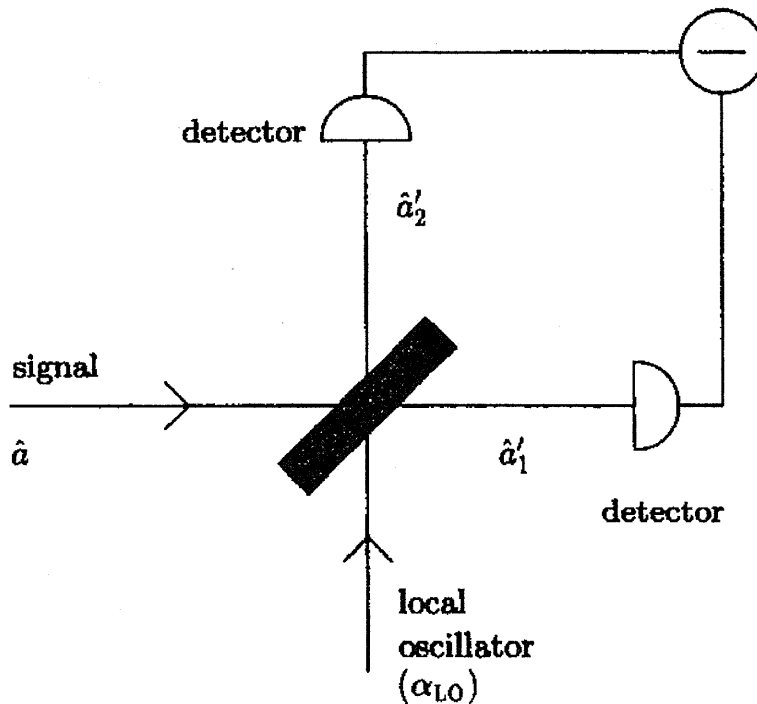


Figure 10. Schematic of a Balanced Homodyne Detector. (courtesy of Ulf Leonhardt)

Furthermore, the balanced homodyne detector is also an amplifier. The LO amplifies the signal by the mutual optical mixing of the two. In other words, the homodyne detector is an interferometer that can be measurably imbalanced by a single photon in the signal mode because the reference field is very intense. A very important technical advantage of this is that the amplified signal is well above the electronic noise floor of the photodiodes. The signal amplitude is enhanced so that even the noisy linear-response photodiodes can detect the quantum features of the signal with single photon resolution. Because the LO serves as a coherent amplifier, it also chooses the signal mode. The LO singles out one spatial-temporal (bosonic) mode from the rest of the continuous quantum field "light" (that matches the LO field). In this way the observer separates the quantum object (a single optical mode) from the rest of the world. The mode function is given by the spatial-temporal shape of the LO beam at the detector surface and during the measurement time interval $[0, T]$. The overall phase and intensity of the LO is comprised in the complex amplitude α_{LO} . Shifting the phase $\theta = \arg(\alpha_{LO})$ rotates the measured \hat{q}_θ . The observer defines via the LO the frame in space and time that is subject to the field-quadrature measurement. By tailoring the shape of the LO beam high spatial-temporal resolution can be achieved.

Photodetection is usually not completely efficient in practice so it is important to describe the influence of inefficiencies on homodyne detection. This is easily done by using the simple model for losses in direct photodetection that was given in Section IIIB-2. We imagine fictitious beam splitters to be placed in front of the two (assumed ideal) detectors in the measurement setup (see Figure 11). We use

$\hat{a}' = \eta^{1/2} \hat{a} + (1-\eta)^{1/2} \hat{a}_2$ from Section IIIB-2 to define the annihilation operators of the detected light modes $\hat{a}_1'' = \eta^{1/2} \hat{a}_1' + (1-\eta)^{1/2} \hat{b}_1$ and $\hat{a}_2'' = \eta^{1/2} \hat{a}_2' + (1-\eta)^{1/2} \hat{b}_2$, where \hat{b}_1 and \hat{b}_2 are the annihilation operators of the vacua entering the second unused ports of the fictitious beam splitters. The annihilation operators \hat{a}_1' and \hat{a}_2' describe the light modes (or fields) emerging from the 50:50 beam splitter where the signal is optically mixed with the LO. Again, the LO is an intense field compared with the signal so it can be treated classically. Therefore, we do some algebra to compute the difference photon number $\hat{n}_{21} = \hat{n}_2'' - \hat{n}_1'' = \hat{a}_2''^\dagger \hat{a}_2'' - \hat{a}_1''^\dagger \hat{a}_1''$, but retain only the leading terms with respect to α_{LO} , and obtain the final result [38]:

$$\hat{n}_{21} = \eta^{1/2} \alpha_{LO}^* \left[\eta^{1/2} \hat{a} + (1-\eta)^{1/2} \hat{b} \right] + HC. \quad (12)$$

The symbol HC in Eq. (12) denotes the Hermitian conjugate of the other part of an expression and $\hat{b} \equiv 2^{-1/2} (\hat{b}_2 - \hat{b}_1)$. The fluctuation mode operator \hat{b} corresponds to the optical mixing of the fictitious vacuum-noise modes \hat{b}_1 and \hat{b}_2 , and it obeys the bosonic commutation relation $[\hat{b}, \hat{b}^\dagger] = 1$ (e.g., see Sect. IIIB-2). Because the interference of vacuum with vacuum yields vacuum, the fluctuation mode \hat{b} can be regarded as a bosonic mode, being in the vacuum state as well.

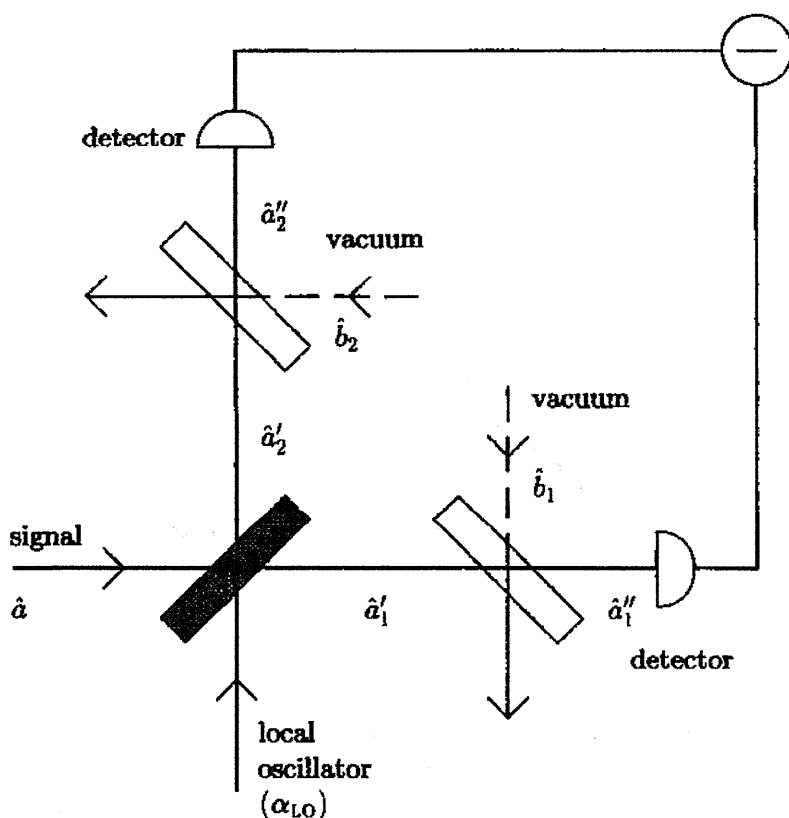


Figure 11. Balanced Homodyne Detector Using Fictitious Beam Splitters to Account for Detection Losses. (courtesy of Ulf Leonhardt)

Equation (12) provides an additional model for detection losses. Similar to direct photon counting, a fictitious vacuum field has to be added to the attenuated signal in homodyne detection. This means that we can replace the arrangement of two fictitious beam splitters in front of the photodetectors with just one effective beam splitter in front of an ideal homodyne detector (see Figure 12). This effective beam splitter accounts for other kinds of losses including mode mismatch, whereby the quantum effects of both detection losses and mode mismatch are comprised in an effective η .

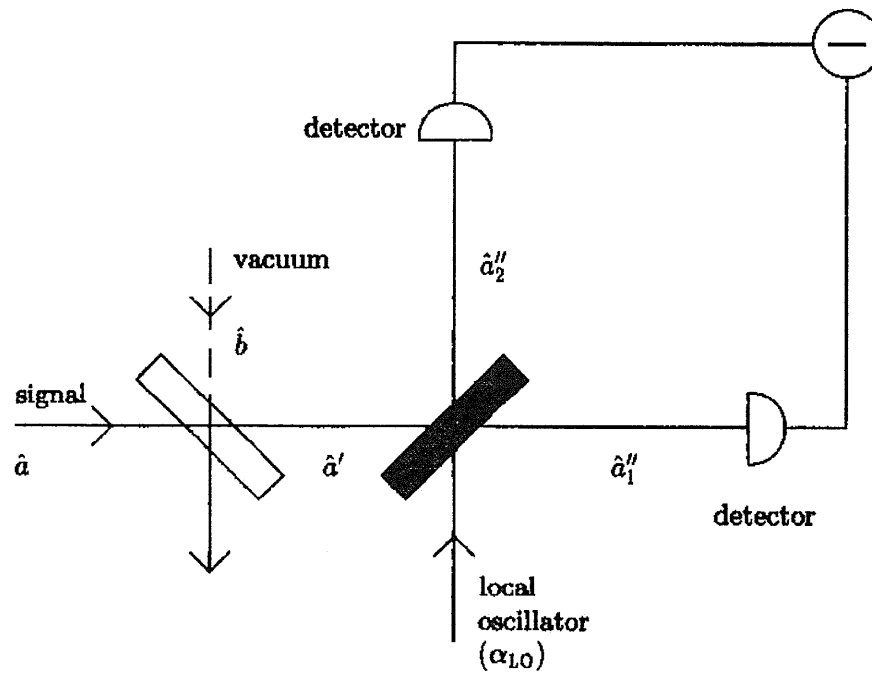


Figure 12. Balanced Homodyne Detector Using A Single Effective Fictitious Beam Splitter to Account for Detection Losses and Mode Mismatch. (courtesy of Ulf Leonhardt)

The consequence of an effective η and Eq. (12) is that the marginal distributions $pr(q, \theta)$ must become a function of the effective η [38]:

$$pr(q, \theta; \eta) = [\pi(1-\eta)]^{-1/2} \int_{-\infty}^{\infty} pr(x, \theta) \exp\left[-\frac{\eta}{1-\eta} (x - \eta^{1/2} q)^2\right] dx, \quad (13)$$

where the $pr(x, \theta)$ inside the integral is defined by Eq. (10) and x is a dummy integration variable. Equation (13) defines the measured quadrature histograms that are used to build the transmission profiles in the tomographic process, which is discussed in the following section.

Outline of Experimental Procedure

The key process of quantum tomography is to picture the “shape” of a quantum object in phase space using the Wigner representation. The marginal distributions [Eq. (10) or (13)] correspond to the tomographic transmission profiles of the Wigner function $W(q, p)$, i.e., to shadows projected onto a line in quantum phase space. Because of the Heisenberg Uncertainty Principle, we cannot measure simultaneously and precisely the position q and the momentum p , and we cannot observe the Wigner function directly as a probability distribution. However, we can measure the quadrature histograms [i.e., the first line in Eq. (10)], and by varying the phase θ we observe the quantum object under different angles. Given the $pr(q, \theta)$, the mathematics of computerized tomography can be applied to deduce the Wigner function.

As discussed in the previous subsection, we can use balanced homodyne detection to precisely measure the quadratures \hat{q}_0 of a spatial-temporal mode. As was also discussed in the previous subsection, the angle θ is defined by the phase of the local oscillator with respect to the signal. The phase θ can be varied using a piezo-electric translator. To measure the quadrature distributions, one may fix θ and perform a series of homodyne measurements at this particular phase to build up a quadrature histogram. Then the LO phase should be changed in order to repeat the procedure at a new phase, and so on. Another possibility is to monitor the phase while it drifts or to sweep it in a known way. In any case, the homodyne measurement must be repeated many times on identically prepared light modes (or on a continuous wave field) to gain sufficient statistical information about the quadrature values at a certain number of reference phases. Finally, the Wigner function is tomographically reconstructed from the experimental data.

It is beyond the scope of this report to summarize the entire subject of experimental quantum tomography, its mathematical basis and procedures of quantum state sampling, and the corresponding algorithms and numerical recipes. The reader should see Reference [58] for the excruciating details.

Balanced homodyne detectors with local oscillators are amplifiers capable of detecting and quantifying vacuum and sub-vacuum fluctuations. This is the subject of the two experimental approaches that will be discussed in the next section.

BALANCED HOMODYNE SYSTEMS FOR MEASURING NEGATIVE (SUB-VACUUM) ENERGY

Time-Domain Balanced Homodyne System

Squeezed states of light, which are "darker than vacuum," have regions with sub-vacuum fluctuations. Slusher and collaborators [40, 41] and Robinson [42, 43] were the first to experimentally observe these sub-vacuum regions. Numerous other experiments followed, which employed variations on the experimental devices and techniques used to generate squeezed light and measure its sub-vacuum fluctuation pulses. Those early experimental devices later gave way to the development and use of balanced homodyne detectors.

For example, Schneider et al. [59] describe their compact and efficient source of amplitude-squeezed light. Their experiment used a semi-monolithic degenerate MgO:LiNbO₃ optical parametric amplifier pumped by a frequency-doubled Nd:YAG laser at 532 nm. They employed injection-seeding of the amplifier by a 1064 nm wave to provide active stabilization of the cavity length and stable operation. At a pump power of 380 mW, their device detected a maximum noise reduction of 6.5 dB in the amplitude fluctuations of the 0.2 mW 1064 nm wave, while the average detected noise reduction in continuous operation over 14 minutes was 6.2 dB. They reported a squeezing of 7.2 dB in the emitted wave.

However, most of these early and more recent series of balanced homodyne detector (BHD) measurements have been performed in the frequency domain. A significant

drawback of this approach is that it reveals information about the quantum state only within the sideband chosen for the measurement. Therefore, the method is incompatible with other techniques for characterizing a quantum state for which such precise selection of spectral modes is impossible. Time-domain BHD resolves this limitation. Hansen et al. [4] describe their experimental time-domain BHD device. They developed a pulsed BHD for precise measurement of the electric field quadratures of pulsed optical quantum states. A high level of common mode suppression (> 85 dB) and low electronic noise (730 electrons per pulse) in their device provides a signal-to-noise ratio of 14 dB for measurement of the quantum noise of individual pulses. Their device achieved a signal-to-noise ratio of 14 dB at a pulse repetition rate of up to 1 MHz, enabling high-accuracy quantum measurements to be carried out in a short time. They performed a quantum tomography of the coherent state as a test for their device, and the Wigner function and density matrix were reconstructed with 99.5% fidelity while their detector exhibited 91% quantum efficiency. Their detection system can also be used for ultrasensitive balanced detection in continuous wave mode. Figure 13 shows a schematic of their time-domain BHD. The figure shows two polarizing beam splitter (PBS) cubes, a 50:50 beam splitter (BS), two half-wave plates ($\lambda/2$), two photodiodes (left-side in dotted box), and the signal processing electronics inside the dotted box.

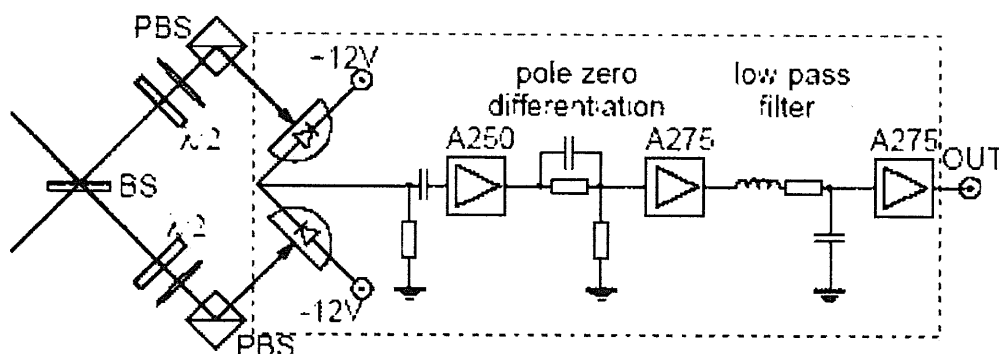


Figure 13. Time-Domain Balanced Homodyne Detector. (courtesy of P. Lodahl)

As we discussed previously in Sections IIIB-4 and IIIB-5, to perform BHD one overlaps on a beam splitter the electromagnetic wave whose quantum state is to be measured and a relatively strong LO wave in the matching optical mode. The two fields emerging from the beam splitter are incident upon two high efficiency photodiodes whose output photocurrents are subtracted. The photocurrent difference is proportional to the value of the electric field operator \hat{E}_θ in the signal mode, where θ is the relative optical phase of the signal and the LO. In traditional frequency-domain BHD, one uses a certain frequency component of the difference signal to determine the quadrature quantum noise of the optical state. The measurement frequency is normally chosen to be approximately 5 to 10 MHz where the technical noise is minimized. Figure 14 shows an example of experimentally measured data for a typical (undisturbed) vacuum state and a squeezed vacuum state using a time-domain BHD system.

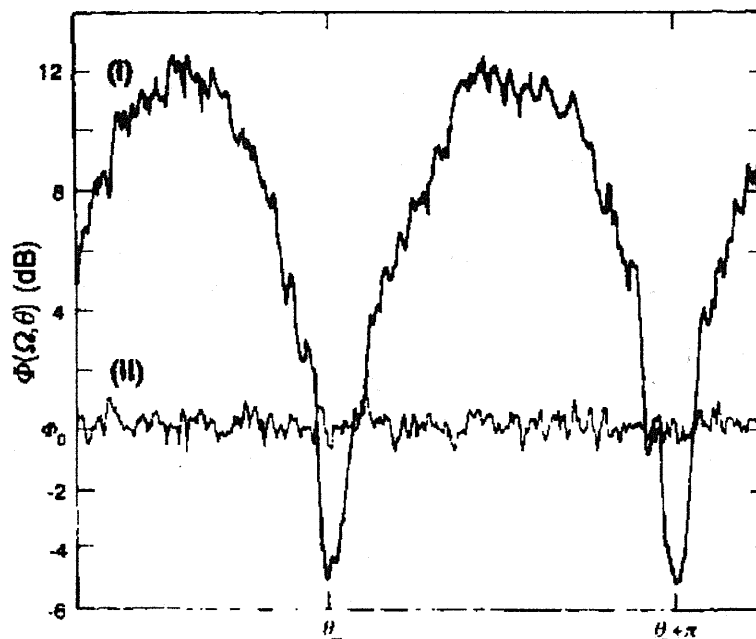


Figure 14. Experimentally Measured Squeezed State. (courtesy of P. Marecki) This graph of vacuum dB noise vs. relative optical phase angle shows an experimentally measured squeezed state (plot (I)) and a normal (undisturbed) vacuum state (plot (II)). The deep valleys with negative dB values in plot (I) are sub-vacuum regions with sub-vacuum (negative) energy density (see also, Figure 1 for a comparison).

When applied to pulsed sources, the frequency-domain BHD technique implies that averaging over many individual laser pulses takes place. However, in time-domain BHD, each laser pulse generates a signal that is observed in real time and yields a single value of a field quadrature. Repeated measurements of a large number of laser pulses produce a quantum probability distribution associated with this quadrature. When transform-limited LO pulses are used, time-domain BHD gives the complete information about the quantum state in the spatial-temporal mode that matches that of the LO.

Hansen et al. [4] point out that time-domain BHD is technically challenging, because 1) the electronics must ensure time resolution of individual laser pulses and 2) the measured quadrature values must not be influenced by low-frequency noise. The detector must provide ultralow noise, high subtraction, and a flat amplification profile in the entire frequency range from DC to at least the LO pulse repetition rate. See Reference [4] for a complete description of their device as shown in Figure 13.

Balanced Homodyne System for Casimir Cavities

What has not been experimentally measured yet are the sub-vacuum fluctuations and their (negative) energy density inside a Casimir cavity. Marecki [5, 6] theoretically evaluated the use of BHDs for this purpose. He proposed that a BHD can be used to detect and spatially map the sub-vacuum fluctuation region inside a Casimir cavity as well as measure its negative energy density spectrum. Marecki discovered that by exploiting a trick with the subtraction of the output of balanced photodiodes, it is possible to quantify the fluctuations of the quantum field (even in the vacuum!), which uniquely addresses Davies and Ottewill's [54] negative energy detector hypothesis.

The quantity of interest (to be measured) is the fluctuations of the quantum electric field $\langle \hat{E}_i(\vec{x}, t) \hat{E}_j(\vec{x}, t) \rangle_S$ (for fields restricted to the frequency ω of the local oscillator) for squeezed and vacuum states, where $\hat{E}_i(\vec{x}, t)$ is the quantum electric field operator (in ground-state representation and restricted in frequencies) at the point \vec{x} , t represents the time-dependence of $\hat{E}_i(\vec{x}, t)$, and $\langle \dots \rangle_S$ stands for the expectation value with respect to an arbitrary initial state S (vacuum, squeezed, ground state, coherent, thermal, etc.) of the quantum radiation field under study. $\langle \hat{E}_i(\vec{x}, t) \hat{E}_j(\vec{x}, t) \rangle_S$ is also called a two-point function. In quantum field theory, the expectation value (or matrix element) computed by inserting a product of two quantum operators between two states, usually the vacuum states, is called a two-point function. This quantity suggests a "relation" between two states in the same dynamics, and it expresses the fluctuations of a quantum field. The product of n -operators is called the n -point function which expresses the higher moments of the quantum field fluctuations.

The goal of the experiment is that a state S of the quantum radiation field under study needs to be characterized by its n -point functions. The typical solution in quantum optics is to use well-characterized quantum systems interacting in a simple way with the quantum radiation field. The detection scheme uses the simple model of a PIN junction photodiode in which a single electron interacts with the quantum radiation field under study. This simple interaction means that the state space of the electron can be severely restricted, the interaction is assumed to be linear in the quantum field, and so the Born approximation can be used [5, 6]. The PIN junction model of the photodetection process is an electron in an initial state $|0\rangle \otimes S$, with its bound-state $|0\rangle$ well-localized around a certain point \vec{x}_0 , that gets excited to the continuum of scattering states $|\vec{q}\rangle$ by the quantum field state of interest S such that the final states of the system are $|\vec{q}\rangle \otimes S$.**** The excitation is caused by the linear (dipole approximation) interaction with the quantum electric field which is

**** The symbol \otimes denotes the tensor product of two quantum eigenstates such that $|a_1, a_2\rangle = |a_1\rangle \otimes |a_2\rangle$ for factorized eigenstates which correspond to independent measurements.

$\hat{H}_{\text{dip-int}} = ex^i \otimes \hat{E}_i(\underline{x}, t) \bullet g(t)$ where e is the electron charge and $g(t)$ is a smooth test (or smearing) function that is equal to 1 during the measurement and smoothly vanishing elsewhere. Using first-order time-dependent perturbation theory, Marecki [5, 6] derived the probability of excitation:

$$P_{\text{exc}}(g, \underline{x}) = \int_{-\infty}^{+\infty} d\tau ds g(\tau)g(s)G^{ij}(\tau-s) \left\langle \hat{E}_i(\underline{x}, \tau) \hat{E}_j(\underline{x}, s) \right\rangle_S, \quad (14)$$

where $G^{ij}(\tau-s) \equiv \int dq \langle 0 | x^i(\tau) | \underline{q} \rangle \langle \underline{q} | x^j(s) | 0 \rangle$ is the electronic two-point function, τ and s are dummy time and integration variables, and $\int d\tau ds g(\tau)g(s)$ is the temporal sensitivity in the measurement process.

The balanced homodyne detector consists of an arrangement of two photodiodes, whose outputs are subtracted, and illuminated with an auxiliary coherent state of the radiation field (i.e., the local oscillator, LO; see Figure 15). Per the discussion in Section IIIB-4, the LO is used as a tool to investigate the properties of a certain state S of the quantum radiation field under study, and so on a BHD the state S is optically mixed with the coherent LO state (see References [5] or [6] for further details). The quantum field S de-balances the detector (stochastic process of measurement). The expectation value of the observable corresponding to the electronic charge collected at the point P in Figure 15 (i.e., the BHD current) is the difference of excitation probabilities of the two photodiodes [5, 6]: $\langle J \rangle_S = P_{\text{exc}}(g, \underline{x}) - P_{\text{exc}}(g, \underline{y})$, where positions \underline{x} and \underline{y} correspond to the positions \underline{x} and \underline{y} in Figure 15. Further calculations and other theoretical considerations lead to the following final result for $\langle J \rangle_S$ [5, 6]:

$$\langle J \rangle_S = \alpha_{el} \bullet \mathcal{E}_{LO}^i \bullet \left\langle \hat{E}_i(\underline{x}, t_0) + \hat{E}_i(\underline{y}, t_0) \right\rangle_S$$

where α_{el} depends on the electronic structure of the PIN semiconductor in the photodiode, \mathcal{E}_{LO}^i is the electric field of the LO (corresponding to F in Figure 15), t_0 is the LO phase that can easily be varied in experiments, and all field operators $\hat{E}_i(\underline{x}, t)$ are restricted to the frequency ω of the LO.

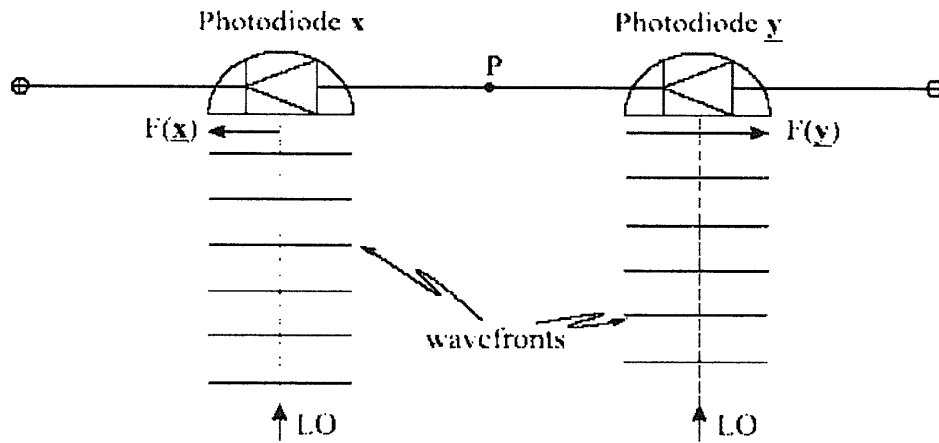


Figure 15. Balanced Homodyne Detector with a Local Oscillator. (courtesy of P. Marecki) The setup is arranged so that the electric field F of the LO at position \underline{x} has a reversed direction with respect to that at position \underline{y} .

If $\langle J \rangle_S$ vanishes, then the variance of the BHD-output is $\langle J^2 \rangle_S$ which provides a characterization of the two-point function of the state S . The variance is [5, 6]:

$$\langle J^2 \rangle_S = \alpha_{et}^2 \bullet E_{LO}^i E_{LO}^j \bullet \left\langle \left[\hat{E}_i(\underline{x}, t_0) + \hat{E}_i(\underline{y}, t_0) \right] \left[\hat{E}_j(\underline{x}, t_0) + \hat{E}_j(\underline{y}, t_0) \right] \right\rangle_S, \quad (15)$$

where $E_{LO}^i E_{LO}^j$ is the power of the LO field. This expression shows that $\langle J^2 \rangle_S$ scales quadratically with the amplitude of the electric field of the quantum state S under study and thus linearly with the power of the LO field. The two-point functions can be quantitatively estimated by performing measurements with different powers of the LO. Therefore, BHDs with local oscillators are amplifiers that are capable of measuring the one- and two-point functions of arbitrary states of quantum fields (even for the vacuum).

For an experimental study of the vacuum state inside a Casimir cavity, the stationary state is specified to be the ground state (Grd) and thus the one-point function $\langle J \rangle_{S=Grd}$ vanishes. For stationary states the $\langle J^2 \rangle_{Grd}$ is related to the spectral density $\sigma_{ij}(\omega, \underline{x}, \underline{y})$ which is defined as the Fourier transform of the two-point function $\langle \hat{E}_i(\underline{x}, t_0) \hat{E}_j(\underline{y}, t_0) \rangle_S$ with respect to time; therefore, we have for ground states [5, 6]:

$$\langle J^2 \rangle_{Grd} = \alpha_{et}^2 \left(E_{LO}^i \right)^2 \int d\omega \sigma_{ij}(\omega, \underline{x}, \underline{y}) \left| \hat{g}(\omega - \omega) \right|^2, \quad (16)$$

where $\hat{g}(\omega)$ is the Fourier transform of $g(t)$ and is sharply peaked around $\omega = 0$. In general, almost all results of quantum field theory in a vacuum state or under the influence of external conditions (i.e., in vacuum states "deformed" by boundary conditions or external fields) are derivable from the spectral density. This quantity is usually known analytically, and it is of great interest to measure it for interesting quantum field states.

Because the ground state is stationary, the quantum noise in the Casimir cavity is time-independent, i.e., it is independent of the phase of the LO, and thus the spectral density is also time-independent. Marecki [5, 6] derived the diagonal part of the spectral density for the y -components of the quantum electric field between two parallel, perfectly conducting plates (positioned at $x = 0$ and $x = a$) in a Casimir cavity (see Figure 2):

$$\sigma_{yy}(\omega, \mathbf{r}, \mathbf{r}) = \frac{\omega^3}{4\pi^2} \sum_{n=-\infty}^{+\infty} [Q(\omega nL) - Q(\omega |2x - nL|)] \quad (17)$$

for $y = 0$, where $L = 2a$ is twice the distance between the plates and the function $Q(x)$ is defined as

$$Q(x) = \frac{\sin x}{x} + \frac{\cos x}{x^2} - \frac{\sin x}{x^3}.$$

Note that the diagonal terms of the spectral density are the important quantities to be measured because they will be dominant if the photodiodes are separated by a sufficiently large distance [5, 6]. Spectral densities reveal much finer details of the quantum ground state than already-measured Casimir forces do. By exploring the freedom of choosing the locations of the photodiodes inside the Casimir cavity as well as the polarizations, phases and frequencies of the LO, one can obtain a detailed characterization of one- and two-point functions of any state S of the quantum electric field. Therefore, an application of this particular type of BHD measurement, via Equations (16) and (17), amounts to a tomography of the ground state of the Casimir cavity.

For the experimental detection of the Casimir spectral density with a BHD-type device, the Casimir cavity plates are separated by $a = 1$ micrometers while the photodiodes inside it are of submicrometer width in the x -direction and submillimeter length in the y -direction (see Figure 16). Photodiodes of several nanometers in size have already been constructed and their high quantum efficiency versions are under development, see Reference [60] and the references cited therein for more technical information. As shown in Figure 16, a coherent state in the TE1 mode of the Casimir cavity with a very small wavenumber in the y -direction provides an appropriate LO. A BHD with such a LO and the photodiodes located as shown in Figure 17 would be sensitive only to the y -component of the quantum electric field. Figure 18 shows a schematic of the BHD apparatus with a LO. In the figure, the linearly polarized signal field S (if present) is optically mixed with a coherent state (LO), which is polarized orthogonally to S , on the polarizing beam splitter (PBS1). The half wave plate (HWP) reflects the planes of polarization with respect to its optical axis, thereby inducing a $\pi/4$ shift of the plane of

polarization of the signal field S . The subsequent PBS2 separates the two orthogonally polarized signals, which are detected at the photodiodes PD x and PD y . The charge collected at point V (corresponding to point P in Figure 15) provides a measure of $\langle J \rangle_{Grd}$ (and its higher moments). Note that the setup is arranged in such a way, that if S happened to be a monochromatic coherent state, then it would be phase-matched to the LO at the point x , but shifted in phase by π at the point y .

Figure 19 displays Marecki's computer model plot of the predicted Casimir spectral density as a function of the distance from the plates x and the frequency ω . For a comparison with quantum optics literature, he plotted the normalized difference between the vacuum and ground state spectral density in the figure (see References [5] and [6] for more detail). Note in the figure that for $\omega < \pi c/a$, the Casimir spectral density vanishes: $\sigma_{Grd}(\omega, \hat{x}, \hat{x}) = 0$, while discontinuities in it appear at $\omega = n\pi c/a$.

Figure 20 displays the corresponding computer model plot by Marecki of the predicted "suppressed" vacuum fluctuations in the ground state relative to "undisturbed" vacuum fluctuations (in absence of the plates) in dB, $10\text{Log}_{10}[\sigma_{Grd}(\omega, \hat{x}, \hat{x})/\sigma_{vac}(\omega, \hat{x}, \hat{x})]$.

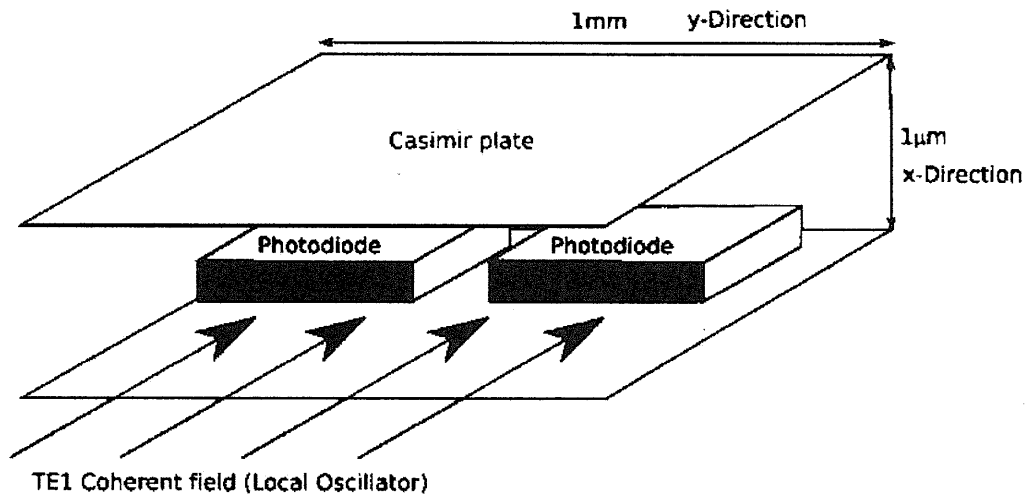


Figure 16. Diagram of Casimir Cavity with BHD Photodiodes. (courtesy of P. Marecki)

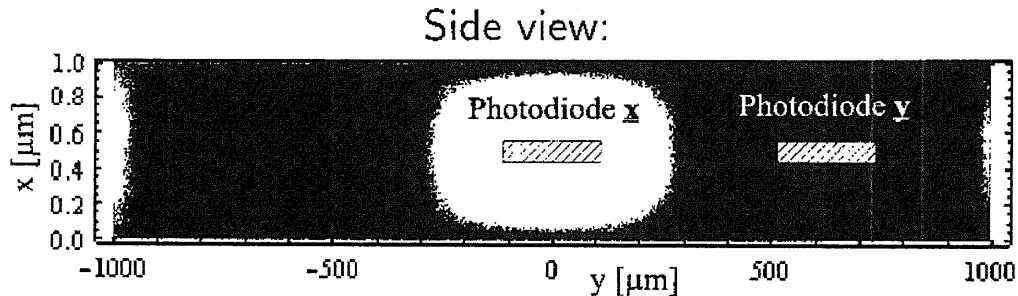


Figure 17. Experimental Setup of BHD Photodiodes and LO Field. (courtesy of P. Marecki) This setup is drawn on the plot of the y -component of the electric field of the TE1 mode of the Casimir cavity. The mode, serving as the LO, propagates in the z -direction perpendicular to the plot.

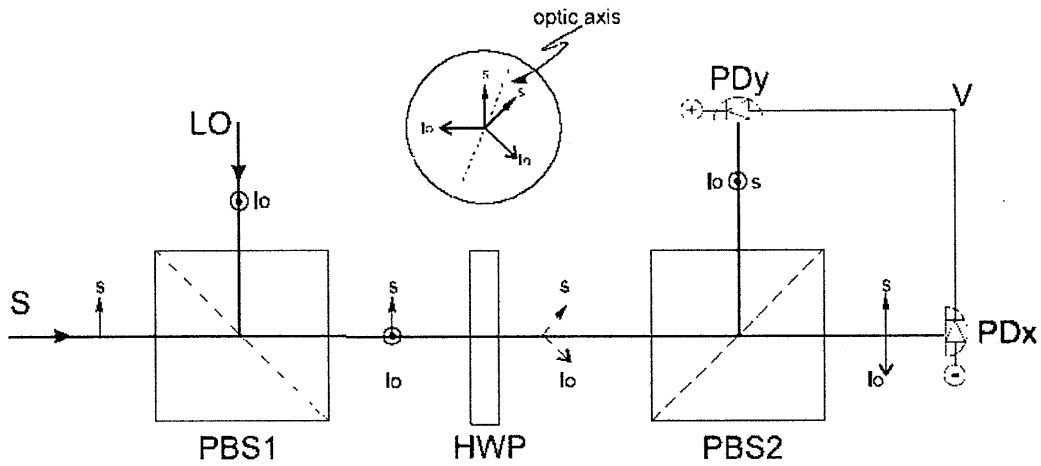


Figure 18. Detailed Schematic of Experimental BHD Apparatus. (courtesy of P. Marecki) Note that point V corresponds to point P in Figure 15.

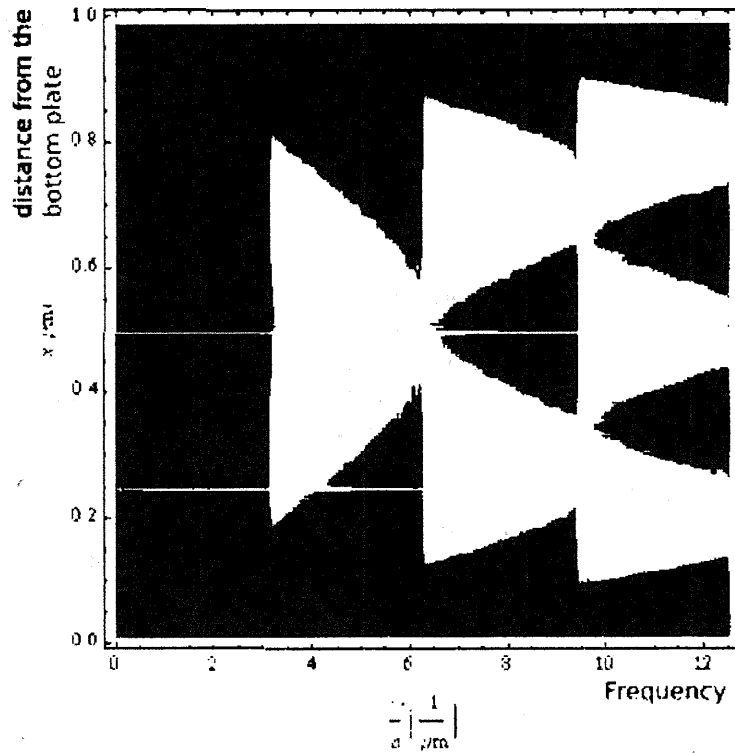


Figure 19. Predicted Casimir Spectral Density σ_{yy} . (courtesy of P. Marecki) σ_{yy} is related to the expected output of a BHD with the LO polarized along the y -direction (parallel to the plates) for the ground state in the Casimir cavity. This is plotted as a function of the position $x \in [0, a]$ between the plates (separation $a = 1 \mu\text{m}$ is assumed) and the frequency $\omega \in [0, 4\pi c/a]$. Negative values (suppression of fluctuations) are shown in deep purple.

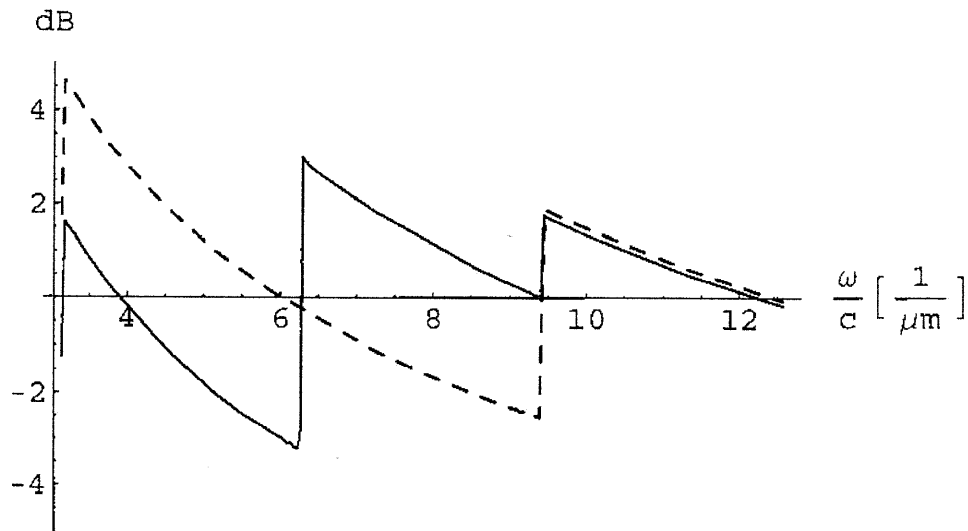


Figure 20. Predicted Suppression of Vacuum Fluctuations in dB. (courtesy of P. Marecki) Vacuum fluctuations in the ground state (for field operators restricted to the frequency ω) relative to vacuum fluctuations (in the absence of the plates) for a BHD at $x = 0.25 \mu\text{m}$ (solid line) and $x = 0.5 \mu\text{m}$ (dashed line) within the cavity. The frequency range is $\omega \in [0, 4\pi c/a]$.

The predicted spectral density pattern shown in Figure 19 is static, i.e., it is independent of the LO phase and in some regions corresponds to the suppression of vacuum fluctuations by at least 3 dB. Such a behavior is allegedly forbidden by a theorem known as the Quantum Inequalities for quantum fields without external conditions (i.e., “undeformed,” or “undisturbed,” vacuum states). The theorem states that regions with sub-vacuum fluctuations must be followed by regions with greatly increased vacuum fluctuations no matter what the state of the quantum field is. This has only been verified for single-mode squeezed light, see, e.g., Figures 1 and 14. A major consequence of this theorem is that sub-vacuum fluctuations, and their corresponding sub-vacuum (negative) energy density, cannot persist for long times. What is surprising here is that Marecki (private communication, Leipzig University, Germany, 2010) claims that the Quantum Inequalities should also apply to the case of static sub-vacuum fluctuations, and their corresponding static sub-vacuum (negative) energy density, inside Casimir cavities. The efficacy of the Quantum Inequalities theorem in its application to curved spacetime physics, and more specifically faster-than-light spacetime geometries, has been argued in the literature in which serious theoretical shortcomings of the theorem have been identified by several investigators (see Reference [1] for the details). Therefore Marecki’s proposed Casimir cavity BHD experiment provides a possible test of yet unexplored generic quantum field theoretic effects in Casimir geometries, complementary to measurements of Casimir forces. We hope that experimental attempts to verify his predictions will follow.

CONCLUSION

Future aerospace platforms may have propulsion systems that modify their surrounding spacetime geometry to implement faster-than-light spaceflight (via traversable wormholes or warp drives) or produce levitation via antigravity. To engineer such a modification of local spacetime requires the use of quantum sub-vacuum fluctuations and their associated sub-vacuum (or negative) energy density. There are two key examples of specially prepared quantum vacuum states that are known to produce small amounts of sub-vacuum (negative) energy density in the laboratory. These are the well-known Casimir effect and squeezed light. There are several other examples of special quantum vacuum states or particle states that produce sub-vacuum (negative) energy density, but they are still under theoretical study.

We already make small amounts of sub-vacuum (negative) energy in the laboratory via the Casimir effect and squeezed light, but we do not yet know if we can access larger amounts for extended periods of time over extended spatial distributions. The Quantum Inequalities theorem suggests that producing large amounts of sub-vacuum (negative) energy in "deformed" vacuum states for extended periods of time in flat or curved spacetimes may not be possible. This claim remains as yet untested by experiment while several investigators have strong arguments showing the theorem is in error in these particular cases.

Quantum optical homodyne tomography can detect and quantify the fluctuations in a variety of ("undisturbed") vacua as well as the sub-vacuum fluctuations found in both squeezed light and Casimir cavities. Squeezed light has time-dependent, alternating regions of sub-vacuum fluctuations (a.k.a. two-point functions) of the quantum electric field. Casimir geometries provide environments with non-trivial position- and frequency-dependent, time-independent, often sub-vacuum fluctuations (two-point functions) of the quantum electric field. Balanced homodyne detectors (BHD) with local oscillators are amplifiers that are capable of providing detailed measurements of the sub-vacuum fluctuations (the two- and n -point functions) of the states of the quantum electromagnetic field.

Nearly a decade ago, Hansen et al. [4] reported on their experimental time-domain (or pulsed) BHD device that they developed to make precise measurements of the quantum electric field quadratures of pulsed optical quantum states (e.g., squeezed light). A master laser produced the local oscillator for this device. The device demonstrated a high level of common mode suppression and low electronic noise, which provided large enough signal-to-noise ratio to measure the quantum noise of individual pulses. The device exhibited over 90% quantum efficiency. However, their device was not designed to directly measure the energy density of the individual pulses. We recommend that a research and development program be implemented to modify the design and operation of the time-domain BHD device in order provide this important data. It will be necessary to develop and commercialize a portable time-domain BHD device for the purpose of detecting, measuring, and spatially mapping the sub-vacuum (negative) energy regions produced by a putative pulsed (or "AC") negative energy generator that might be used for engineering the spacetime surrounding an aerospace platform for propulsion purposes. A number of modified time-domain BHD devices could also be assembled in a sensor array for surveillance and detection of any anomalous aerospace platforms that might use engineered spacetime effects for propulsion.

What has not been experimentally measured yet are the sub-vacuum fluctuations and their corresponding sub-vacuum (negative) energy density inside a Casimir cavity. Casimir cavities produce static, or time-independent, sub-vacuum fluctuations and (negative) energy density. Marecki [5, 6] proposed a modified BHD and computed the two-point function and the associated spectral density for the ground state of the quantum electric field in Casimir geometries, and predicted a position- and frequency-dependent pattern of BHD responses if a device of this type is placed inside a Casimir cavity. He discovered that by exploiting a trick with the subtraction of the output of two balanced photodiodes, it is possible to quantify and map the sub-vacuum fluctuations of the quantum field and its corresponding energy density inside the cavity. His modified BHD design uses the electric field of the TE₁ mode of the Casimir cavity as the local oscillator. Marecki also discovered that the sub-vacuum (negative) energy density regions inside a Casimir cavity violate the Quantum Inequalities theorem. We recommend that an experimental program be implemented to test Marecki's modified BHD and his predictions for Casimir geometries. Using this device to also test the efficacy of the Quantum Inequalities theorem is a necessary part of the proposed experimental program. If such experiments are successful, then it will be necessary to follow up by implementing a program to develop and commercialize a portable "modified-Marecki BHD" device for the purpose of detecting, measuring, and spatially mapping the sub-vacuum (negative) energy regions produced by a putative static (or "DC") negative energy generator that would be used for engineering the spacetime surrounding an aerospace platform for propulsion purposes. Because the Casimir effect and its associated negative energy are incredibly feeble, such putative propulsion systems will not involve the use of Casimir cavities to produce a free-space distribution of negative energy surrounding the platform. Therefore, a modified-Marecki BHD will require a high quality laser for the local oscillator and the photodiodes are allowed to be much larger in size. A number of modified-Marecki BHD devices could also be assembled in a sensor array for surveillance and detection of any anomalous aerospace platforms that might use engineered spacetime effects for propulsion.

ACKNOWLEDGEMENTS

The author would like to thank Professors Ulf Leonhardt and Piotr Marecki for contributing their lecture notes, references, and experimental data to the contents of this report.

REFERENCES

- [1] Davis, E. W. (2009), "Faster-Than-Light Approaches in General Relativity," in *Frontiers of Propulsion Science*, eds. M. G. Millis and E. W. Davis, Progress in Astronautics & Aeronautics Series, Vol. 227, American Institute of Aeronautics & Astronautics Press, Reston, VA, pp. 473-509.
- [2] Davis, E. W. (2009), "Gravity Control within Newtonian and General Relativity Physics," in *Frontiers of Propulsion Science*, eds. M. G. Millis and E. W. Davis, Progress in Astronautics & Aeronautics Series, Vol. 227, American Institute of Aeronautics & Astronautics Press, Reston, VA, pp. 175-227.
- [3] Epstein, H., Glaser, V., and Jaffe, A. (1965), "Nonpositivity of the Energy Density in Quantized Field Theories," *Nuovo Cimento*, Vol. 36, pp. 1016-1022.
- [4] Hansen, H., et al. (2001), "Ultrasensitive pulsed, balanced homodyne detector: application to time-domain quantum measurements," *Optics Letters*, Vol. 26, pp. 1714-1716.
- [5] Marecki, P. (2008), "Balanced homodyne detectors and Casimir energy densities," *Journal of Physics A: Mathematical and Theoretical*, Vol. 41, 164037.
- [6] Marecki, P. (2008), "Balanced homodyne detectors in quantum field theory," *Physical Review A*, Vol. 77, 012101.
- [7] Ford, L. H., and Roman, T. A. (2003), "Negative Energy, Wormholes and Warp Drive," *Scientific American*, Vol. 13, pp. 84-91.
- [8] Morris, M. S., and Thorne, K. S. (1988), "Wormholes in spacetime and their use for interstellar travel: A tool for teaching general relativity," *American Journal of Physics*, Vol. 56, pp. 395-412.
- [9] Visser, M. (1995), *Lorentzian Wormholes: From Einstein to Hawking*, AIP Press, New York.
- [10] Hawking, S. W., and Ellis, G. F. R. (1973), *The Large-Scale Structure of Space-Time*, Cambridge Univ. Press, Cambridge, UK, 1973, pp. 88-91, 95-96.
- [11] Visser, M. (1990), "Wormholes, baby universes, and causality," *Physical Review D*, Vol. 41, pp. 1116-1124.
- [12] Visser, M. (1996), "Gravitational vacuum polarization. I. Energy conditions in the Hartle-Hawking vacuum," *Physical Review D*, Vol. 54, pp. 5103-5115.
- [13] Visser, M. (1996), "Gravitational vacuum polarization. II. Energy conditions in the Boulware vacuum," *Physical Review D*, Vol. 54, pp. 5116-5122.
- [14] Visser, M. (1996), "Gravitational vacuum polarization. III. Energy conditions in the (1+1)-dimensional Schwarzschild spacetime," *Physical Review D*, Vol. 54, pp. 5123-5128.
- [15] Visser, M. (1997), "Gravitational vacuum polarization. IV. Energy conditions in the Unruh vacuum," *Physical Review D*, Vol. 56, pp. 936-952.
- [16] Barcelo, C., and Visser, M. (2002), "Twilight for the energy conditions?," *International Journal of Modern Physics D*, Vol. 11, pp. 1553-1560.
- [17] Herrmann, F. (1989), "Energy Density and Stress: A New Approach to Teaching Electromagnetism," *American Journal of Physics*, Vol. 57, pp. 707-714.
- [18] Drummond, P. D., and Ficek, Z., eds. (2004), *Quantum Squeezing*, Springer-Verlag, Berlin.
- [19] Hochberg, D., and Kephart, T. W. (1991), "Lorentzian wormholes from the gravitationally squeezed vacuum," *Physics Letters B*, Vol. 268, pp. 377-383.
- [20] DeWitt, B. S. (1975), "Quantum Field Theory in Curved Spacetime," *Physics Reports*, Vol. 19C, pp. 295-357.
- [21] DeWitt, B. S. (1979), "Quantum gravity: the new synthesis," *General Relativity: An Einstein Centenary Survey*, edited by S. W. Hawking and W. Israel, Cambridge Univ. Press, Cambridge, UK, pp. 680-745.
- [22] DeWitt, B. S. (1989), "The Casimir Effect in Field Theory," *Physics in the Making, Essays on Developments in 20th Century Physics, In Honour of H. B. G. Casimir*, edited by A. Sarlemijn and J. Sparnaay, North-Holland Elsevier Science Publ., New York, pp. 247-272.
- [23] Birrell, N. D., and Davies, P. C. W. (1984), *Quantum fields in curved space*, Cambridge Univ. Press, Cambridge, UK.
- [24] Saunders, S., and Brown, H. R., eds. (1991), *The Philosophy of Vacuum*, Clarendon Press, Oxford.
- [25] Milonni, P. W. (1994), *The Quantum Vacuum: An Introduction to Quantum Electrodynamics*, Academic Press, New York, Chapters 1, 2, and 8.
- [26] Milton, K. A. (2001), *The Casimir Effect: Physical Manifestations of Zero-Point Energy*, World Scientific, New Jersey.
- [27] Mostepanenko, V. M., and Trunov, N. N. (2007), *The Casimir Effect and its Applications*, Oxford University Press, Oxford.
- [28] Bordag, M., et al. (2009), *Advances in the Casimir Effect*, Oxford University Press, Oxford.
- [29] Vollick, D. N. (1998), "Negative energy density states for the Dirac field in flat spacetime," *Physical Review D*, Vol. 57, pp. 3484-3488.
- [30] Yu, H., and Shu, W. (2003), "Quantum states with negative energy density in the Dirac field and quantum inequalities," *Physics Letters B*, Vol. 570, pp. 123-128.
- [31] Alcubierre, M. (1994), "The warp drive: hyper-fast travel within general relativity," *Classical and Quantum Gravity*, Vol. 11, pp. L73-L77.
- [32] Olum, K. D. (1998), "Superluminal Travel Requires Negative Energies," *Physical Review Letters*, Vol. 81, pp. 3567-3570.
- [33] Gao, S., and Wald, R. M. (2000), "Theorems on gravitational time delay and related issues," *Classical and Quantum Gravity*, Vol. 17, pp. 4999-5008.

- [34] Morris, M. S., Thorne, K. S., and Yurtsever, U. (1988), "Wormholes, time machines, and the weak energy conditions," *Physical Review Letters*, Vol. 61, pp. 1446-1449.
- [35] Ford, L. H. (1978), "Quantum coherence effects and the second law of thermodynamics," *Proceedings of the Royal Society of London. Series A, Mathematical and Physical Sciences*, Vol. 364, pp. 227-236.
- [36] Davies, P. C. W. (1982), "Can moving mirrors violate the second law of thermodynamics?," *Physics Letters B*, Vol. 11, p. 215.
- [37] Everett, A. E. (1996), "Warp drive and causality," *Physical Review D*, Vol. 53, pp. 7365-7368.
- [38] Gerry, C. C., and Knight, P. L. (2005), *Introductory Quantum Optics*, Cambridge University Press, New York.
- [39] Mulliken, R. S. (1924), "The Band Spectrum of Boron Monoxide," *Nature*, Vol. 114, p. 349.
- [40] Slusher, R. E., et al. (1985), "Observation of Squeezed States Generated by Four-Wave Mixing in an Optical Cavity," *Physical Review Letters*, Vol. 55, pp. 2409-2412.
- [41] Slusher, R. E., and Yurke, B. (1986), "Squeezed Light," *Scientific American*, Vol. 254, pp. 50-56.
- [42] Robinson, A. L. (1985), "Bell Labs Generates Squeezed Light," *Science*, Vol. 230, pp. 927-929.
- [43] Robinson, A. L. (1986), "Now Four Laboratories Have Squeezed Light," *Science*, Vol. 233, pp. 280-281.
- [44] Saleh, B. E. A., and Teich, M. C. (1991), *Fundamentals of Photonics*, Wiley Series in Pure and Applied Optics, John Wiley & Sons, Inc., New York, pp. 414-416.
- [45] Caves, C. M. (1981), "Quantum-mechanical noise in an interferometer," *Physical Review D*, Vol. 23, pp. 1693-1708.
- [46] Pfenning, M. J. (1998), "Quantum Inequality Restrictions on Negative Energy Densities in Curved Spacetimes," Ph.D. Dissertation, Dept. of Physics and Astronomy, Tufts Univ., Medford, MA.
- [47] Casimir, H. B. G., "On the Attraction Between Two Perfectly Conducting Plates," *Proc. Kon. Ned. Akad. Wetensch.*, Vol. 51, 1948, pp. 793-796.
- [48] Lamoreaux, S. K., "Demonstration of the Casimir Force in the 0.6 to 6 μm Range," *Physical Review Letters*, Vol. 78, 1997, pp. 5-8.
- [49] Mohideen, U., "Precision Measurement of the Casimir Force from 0.1 to 0.9 μm ," *Physical Review Letters*, Vol. 81, 1998, pp. 4549-4552.
- [50] Chen, F., et al., "Theory confronts experiment in the Casimir force measurements: Quantification of errors and precision," *Physical Review A*, Vol. 69, 2004, 022117.
- [51] Brown, L. S., and Maclay, G. J., "Vacuum Stress between Conducting Plates: An Image Solution," *Physical Review*, Vol. 184, 1969, pp. 1272-1279.
- [52] Walker, W. R., "Negative energy fluxes and moving mirrors in curved space," *Classical and Quantum Gravity*, Vol. 2, 1985, pp. L37-L40.
- [53] Moore, G. T., "Quantum Theory of the Electromagnetic Field in a Variable-Length One-Dimensional Cavity," *Journal of Mathematical Physics*, Vol. 11, 1970, pp. 2679-2691.
- [54] Davies, P. C. W., and Ottewill, A. C., "Detection of negative energy: 4-dimensional examples," *Physical Review D*, Vol. 65, 2002, 104014.
- [55] Neergaard-Nielsen, J. S., et al. (2006), "Generation of a Superposition of Odd Photon Number States for Quantum Information Networks," *Physical Review Letters*, Vol. 97, 083604.
- [56] Ourjoumtsev, A., et al. (2006), "Generating Optical Schrödinger Kittens for Quantum Information Processing," *Science*, Vol. 312, pp. 83-86.
- [57] Mandel, L., and Wolf, E. (1995), *Optical Coherence and Quantum Optics*, Cambridge University Press, Cambridge, UK, Section 17.2.
- [58] Leonhardt, U. (1997), *Measuring the Quantum State of Light*, Cambridge Studies in Modern Optics, Cambridge University Press, Cambridge, UK, pp. 98-143.
- [59] Schneider, K., et al. (1998), "Generation of strongly squeezed continuous-wave light at 1064 nm," *Optics Express*, Vol. 2, Issue 3, pp. 59-64.
- [60] Collin, S., Pardo, F., and Pelouard, J.-L. (2003), "Resonant-cavity-enhanced subwavelength metal semiconductor-metal photodetector," *Applied Physics Letters*, Vol. 83, pp. 1521-1523.